Comprehensive 4E assessment of diesel exhaust waste heat recovery for domestic water preheating using a concentric-tube heat exchanger

Rassol Hamed Rasheed, Samer Ali, Ahmed Mohsin Alsayah, Mohammed Alshukri, Saif Ali Kadhim, Jalal Faraj, Cathy Castelain, Marwan Fahs, Mahmoud Khaled

Energy Conversion and Management: X 30 (2026) 101731

Contents lists available at ScienceDirect

Energy Conversion and Management: X

journal homepage: www.sciencedirect.com/journal/energy-conversion-and-management-x

Comprehensive 4E assessment of diesel exhaust waste heat recovery for domestic water preheating using a concentric-tube heat exchanger

Rassol Hamed Rasheed [a,b], Samer Ali [c], Ahmed Mohsin Alsayah [d], Mohammed J. Alshukri [e], Saif Ali Kadhim [f], Jalal Faraj [g,h], Cathy Castelain [i], Marwan Fahs [j,*], Mahmoud Khaled [g,k,*]

[a] Air-conditioning and Refrigeration Engineering Techniques Department, College of Engineering, University of Warith Al-Anbiyaa, Iraq
[b] Department of Renewable Energy Techniques, Karbala Technical Institute, Al-Furat Al-Awsat Technical University (ATU), Karbala, Iraq
[c] Univ. Lille, Institut Mines-Télécom, Univ. Artois, Junia, ULR 4515 – LGCgE, Laboratoire de Génie Civil et géo-Environnement, F-59000 Lille, France
[d] Refrigeration and Air-conditioning Department, Technical Engineering College, The Islamic University, Najaf, Iraq
[e] Department of Mechanical Engineering, Faculty of Engineering, Kufa University, 54002 Najaf, Iraq
[f] Mechanical Engineering Department, University of Technology - Iraq, Baghdad, Iraq
[g] Energy and Thermo-Fluid Group, Lebanese International University (LIU), Bekaa, Lebanon
[h] Energy and Thermo-Fluid Group, The International University (IU), Mount Lebanon, Lebanon
[i] Nantes Université, CNRS, Laboratoire de thermique et energie de Nantes (LTeN), UMR6607, 44000 Nantes, France
[j] Université de Strasbourg, CNRS, ENGEES, Institut Terre et Environnement de Strasbourg, UMR 7063, F-67000 Strasbourg, France
[k] GUST Center for Sustainable Development, Gulf University for Science and Technology, Kuwait

ARTICLE INFO

Keywords:
Waste-heat recovery
Diesel exhaust
Concentric-tube heat exchanger
4E assessment
Domestic hot water
Sustainability

ABSTRACT

Recovering low-to-medium grade waste heat from diesel-engine exhaust to preheat domestic hot water (DHW) can reduce auxiliary heating demand; however, published exhaust-to-water recovery studies commonly emphasize first-law gains while providing limited second-law quantification under coupled variations of flow conditions and concentric-tube geometry, and rarely integrate pumping-power penalties with discounted economic indicators and life-cycle-based environmental metrics in a unified framework. To address this gap, this work proposes a comprehensive 4E (energy–exergy–exergoeconomic–exergoenvironmental) assessment of a counter-flow heat-recovery concentric-tube heat exchanger (HR-CTHE) integrated upstream of an auxiliary water heater. The thermo-hydraulic model combines a validated overall-U correlation with developing-flow correction and a counter-flow ε–NTU formulation with temperature-dependent properties, alongside regime-dependent pumping-power prediction. A broad parametric sweep is conducted over exhaust inlet temperature ($T_{h,i}$ = 500–900 K), Reynolds numbers ($\mathrm{Re}_h, \mathrm{Re}_c = 10^3$–$2 \times 10^4$), inner diameter ($D_i$ = 0.03–0.15 m), and diameter ratio (D_o/D_i = 1.25–3), for DHW setpoints of 338–365 K and a 4 m exchanger. Results show that recovered heat rate is primarily governed by $T_{h,i}$ and hot-side turbulence (increasing Re_h yields the strongest gains), whereas the temperature lift of the recovered stream is maximized at moderated cold-side flow rates; thus, conditions that maximize q do not necessarily maximize the recovered-water outlet temperature. Exergetic efficiencies remain intrinsically low for this low-grade recovery application and deteriorate when Re_c is increased excessively due to amplified entropy generation and pumping penalties, highlighting the importance of hot-side strengthening combined with cold-side moderation. The discounted economic analysis (annual savings, NPV, and discounted payback over 10 years at 10% discount rate) indicates that profitability is substantially higher when displacing electricity than natural gas, and is favored by tight annular gaps ($D_o/D_i \approx 1.25$), high $T_{h,i}$, and sufficiently large Re_h. Finally, Eco-indicator 99-based exergoenvironmental accounting shows that the HR-CTHE reduces life-cycle impact mainly by lowering auxiliary heating demand; avoided impacts increase with $T_{h,i}$ and appropriate flow balancing, while very high Re_c can partially offset benefits through higher pumping requirements. Overall, the proposed 4E framework delivers performance maps and actionable operating/design guidelines for exhaust-to-DHW preheating using compact concentric-tube recovery systems.

* Corresponding authors.
E-mail addresses: fahs@unistra.fr (M. Fahs), mahmoud.khaled@liu.edu.lb (M. Khaled).

https://doi.org/10.1016/j.ecmx.2026.101731
Received 11 January 2026; Received in revised form 17 February 2026; Accepted 3 March 2026
Available online 14 March 2026

1. Introduction

The ongoing global energy crisis and rising fuel prices have increased the urgency of reducing energy consumption and lowering operational costs across various sectors [1–4]. In the pursuit of sustainability, recent research has emphasized the importance of green building materials to reduce carbon footprints [5] and the implementation of zero-energy strategies in mixed-use buildings to minimize grid reliance [6]. In domestic and commercial settings, water heating remains an energy-intensive process, often accounting for a substantial share of total energy usage. According to international energy statistics, water heating can represent up to 20% of a household's energy consumption [7]. As conventional energy resources become more scarce and expensive, improving the efficiency and sustainability of water heating systems is a critical challenge [8–11].

One effective approach to addressing this challenge is the development of heat recovery systems that capture and reuse waste heat [12–15]. Instead of relying solely on primary energy sources, these systems recover thermal energy that would otherwise be lost, reducing fuel consumption and lowering costs [16–18]. This approach aligns with broader optimization efforts in the energy sector, such as optimizing economic-technical models for hydrogen production and waste-to-energy conversion [19]. Several heat recovery technologies have been studied. For instance, drain water heat recovery systems are used in residential settings to preheat cold water using heat from wastewater streams [20,21]. Similarly, industrial facilities implement waste heat boilers or economizers to improve efficiency by recovering heat from flue gases before they are discharged into the environment [22,23].

For water heating applications, numerous studies have examined the feasibility of integrating heat exchangers into domestic hot water supply systems. Recent bibliometric analyses of thermal energy storage indicate a growing global trend toward optimizing these thermal systems for building applications [24]. Advanced simulation tools have been instrumental in this progress; for example, TRNSYS has been effectively used to model performance in solar thermal desalination systems [25], and techno-economic simulations have been applied to solar flat plate collectors to meet building hot water demand [26]. Building on these methodologies, significant energy savings can be achieved by utilizing low-grade thermal energy sources. Zhang et al. [27] analyzed the efficiency of a horizontal drain water heat recovery (DWHR) system for residential high-rise buildings, demonstrating energy efficiencies of 90%–95% and heating energy savings of approximately 15% compared to conventional systems. Jia and Lee [28] introduced the storage-enhanced heat recovery room air-conditioner (SEHRAC) for domestic hot water heating in dense urban areas, achieving a potential 9.3% reduction in residential energy consumption. Similarly, Piotrowska and Słys [29] evaluated a novel horizontal heat exchanger for gray water recovery, reporting energy demand reductions of 22%–31% with payback periods ranging from 4 to 9 years for electric water heaters and at least 12 years for gas heaters.

Among the many available waste heat sources, exhaust gas from internal combustion engines (ICEs), such as those in diesel generators, offer a significant opportunity for heat recovery. These exhaust streams reach high temperatures and contain substantial recoverable energy [30,31]. Recent research has explored integrating compact heat exchangers directly into exhaust lines to capture this energy efficiently. Ganesh et al. [32] studied phase change materials (PCMs) for thermal energy storage in diesel engine exhausts, reducing heat loss to the atmosphere from 45.1% to 39.5% and storing 5.5% of total energy for reuse. Gholizadeh et al. [33] examined hybrid nanofluids and fin modifications in shell-and-tube heat exchangers, achieving a 7% reduction in exhaust gas temperature and a 64% increase in heat transfer rates. Ni et al. [34] developed a compact thermoelectric generator (TEG) system for diesel engine exhausts, yielding a peak power output of 80.9 W and a thermoelectric efficiency of 2.1%. Orido et al. [35] analyzed a hybrid recuperative heat exchanger for diesel engine exhaust heat recovery, raising greenhouse dryer temperatures by 11.78°C and reducing drying time.

To position the present contribution and make the research gap explicit, Table 1 compares representative waste-heat recovery studies (including diesel/ICE exhaust recovery and DHW-related recovery) and highlights the analysis scope and key parameters considered.

Despite these advances, Table 1 reveals three specific gaps for diesel-exhaust-to-water recovery systems intended for domestic hot-water (DHW) use: (i) many studies emphasize energy recovery but do not provide a systematic second-law quantification of irreversibilities under combined variations of hot/cold flow conditions and exchanger geometry; (ii) economic evaluations are often limited (e.g., without discounted cash-flow metrics such as NPV and discounted payback, and without contrasting electricity vs. natural-gas baselines), and pumping-power penalties are not consistently integrated; and (iii) life-cycle-based environmental indicators are rarely coupled to an exergy framework, which obscures trade-offs between recovered heat, auxiliary energy savings, and embodied impacts.

Accordingly, the innovation of this work is a unified 4E framework for a counter-flow heat-recovery concentric-tube heat exchanger (HR-CTHE) for DHW preheating, combining a validated predictive model for heat transfer and pumping power with discounted economic indicators and Eco-indicator 99-based exergoenvironmental metrics over a broad parametric space. Specifically, this paper:

- develops a coupled energy/exergy model using a validated overall-U correlation with a developing-flow correction and an ε–NTU formulation;
- quantifies pumping-power penalties consistently across laminar and turbulent regimes on both sides;
- evaluates profitability using annual savings, NPV, and discounted payback period for both electricity and natural-gas displacement;
- couples the thermodynamic model with life-cycle impact factors to compute environmental impact rates and avoided impacts; and
- provides performance maps and sensitivity trends to identify dominant levers ($T_{h,i}$ and Re_h) and design guidance (tight annular gap and moderated cold-side flow).

The remainder of the paper is structured as follows: 2 describes the problem setup and the selected heat recovery configuration, along with the investigated parameters. 3 presents the mathematical models and correlations used to predict heat transfer rates and pumping power consumption. The results are discussed in 4, highlighting key trends and providing insights into optimal design strategies. Finally, 5 summarizes the main findings and provides recommendations for optimal operation.

2. Problem description

To efficiently harness waste heat from diesel engine exhaust gas for domestic water heating, a practical and effective heat exchanger design is essential. In this study, we have chosen a heat recovery counter-flow concentric tube heat exchanger (HR-CTHE) for this purpose, as depicted in Fig. 1. Several key factors influenced this selection.

Firstly, the concentric tube heat exchanger is renowned for its simplicity and cost-effectiveness, making it ideal for residential applications. Its straightforward design eases manufacturing, installation, and maintenance processes, which is crucial for widespread adoption in home settings. The compactness of the concentric arrangement also conserves space—a significant advantage in residential environments where space is often limited.

Secondly, employing a counter-flow configuration enhances heat transfer efficiency by maximizing the temperature difference between the hot exhaust gas and the cold water along the entire length of the exchanger. In this arrangement, the coldest water meets the hottest exhaust gas, maintaining a high temperature gradient that promotes efficient heat exchange. This results in a higher logarithmic mean

Table 1
Positioning of the present study relative to representative waste-heat recovery works and the present contribution.

Reference	Heat source	Technology/HX	E	Ex	Econ	Env	Main varied parameters/key outcomes (as reported)
Zhang et al. [27]	Drain/gray water	Horizontal DWHR HX	✓	–	–	–	Energy efficiency and savings reported
Jia & Lee [28]	Room AC waste heat	SEHRAC + storage	✓	–	–	–	Storage-enhanced recovery for DHW
Piotrowska & Słys [29]	Gray water	Horizontal HX	✓	–	✓	–	Payback and energy reductions reported
Ravichandran et al. [21]	Drain water	DWHR	✓	–	✓	–	Feasibility and performance indicators
Ganesh et al. [32]	Diesel exhaust	PCM-based recovery	✓	–	–	–	Exhaust recovery + thermal storage metrics
Gholizadeh et al. [33]	Diesel exhaust	Shell-and-tube (fins/nanofluid)	✓	–	–	–	Heat-transfer enhancement strategies
Ni et al. [34]	Diesel exhaust	Thermoelectric generator	✓	–	–	–	Power output and efficiency reported
Orido et al. [35]	Diesel exhaust	Recuperative HX (dryer)	✓	–	–	–	Temperature rise and drying impact
Xie et al. [30]	ICE exhaust	WHR optimization study	✓	✓	✓	–	Optimization with thermodynamic/economic indicators
Varshil et al. [31]	ICE exhaust	WHR assessment	✓	✓	–	–	Comparative WHR performance indicators
Present work	Diesel exhaust → water	Counter-flow HR-CTHE + auxiliary heater	✓	✓	✓	✓	Wide sweep in $T_{h,i}$, Re_h, Re_c, D_i, D_o/D_i; pumping penalty included; NPV/DPP; LCA-based avoided impact

temperature difference (LMTD), which is beneficial for maximizing the amount of heat recovered.

The primary application of the recovered heat is to preheat cold water for domestic uses such as showers, sinks, and other household needs. By preheating the water using the waste heat from exhaust gas, the energy demand on auxiliary water heaters is reduced, leading to significant energy savings and lower utility costs for homeowners.

To thoroughly evaluate the HR-CTHE's performance under various realistic conditions, we consider a range of operating parameters:

Reynolds numbers

- **Exhaust Gas**: The Reynolds number for the hot exhaust gas (Re_h) is varied at five levels—1000; 2000; 4000; 10,000; and 20,000. This range covers both laminar and turbulent flow regimes typical of different engine operating conditions.
- **Cold Water**: Similarly, the Reynolds number for the cold water (Re_c) is varied at the same five levels to represent different flow rates that might occur in domestic water systems.

Inlet temperatures

- **Exhaust Gas**: Inlet temperatures of 500 K, 700 K, and 900 K are considered for the exhaust gas. These temperatures were selected to represent the typical range of Diesel engine exhaust temperatures observed under low, medium, and high-load operating conditions, consistent with reported experimental data [30,32].
- **Cold Water**: The cold water inlet temperature ($T_{c,i}$) is fixed at 280 K, representing a standard annual average temperature for domestic municipal water supply [20].

Inner diameters and diameter ratios

- **Inner Diameters**: Three inner diameters D_i for the inner tube are selected — 0.03 m, 0.06 m, and 0.15 m — to examine the impact of size on heat transfer performance.
- **Diameter Ratios**: Corresponding outer tube diameters D_o are determined using diameter ratios D_o/D_i of 1.25, 1.5, and 3. This allows us to assess how the proportion between the inner and outer tubes affects the heat exchanger's efficiency.

Heat exchanger length

The length of the HR-CTHE L is fixed at 4 m for all configurations. This length provides a balance between sufficient heat transfer surface area and practical size for residential installation.

Target outlet temperatures

We aim for three target outlet temperatures for the preheated water at the outlet of the auxiliary water heater ($T_{c,o}$): 338 K (65°C), 353 K (80°C), and 365 K (92°C). These temperatures cover a range of domestic hot water requirements:

- **338 K (65°C)**: Suitable for general household activities like bathing and handwashing.
- **353 K (80°C)**: Ideal for applications requiring hotter water, such as dishwashing and laundry.
- **365 K (92°C)**: Applicable for specialized household needs that demand higher temperatures.

By studying these parameters, we can evaluate how effectively the HR-CTHE can preheat cold water and reduce the energy required from auxiliary heaters, thereby enhancing overall energy efficiency.

System configuration overview

Fig. 1(a) illustrates the conventional domestic water heating system without heat recovery. In this setup, cold water at inlet temperature $T_{c,i}$ is heated directly to the desired temperature $T_{c,o}$ by an auxiliary heater powered by electricity or natural gas.

Fig. 1(b) shows the system integrated with the HR-CTHE. Here:

- Hot exhaust gas from the Diesel engine, at inlet and outlet temperatures $T_{h,i}$ and $T_{h,o}$, and mass flow rate $\dot{m}_h$, flow through the inner tube of the heat exchanger.
- Cold water at temperature $T_{c,i}$ and mass flow rate $\dot{m}_c$ flows counter-currently through the outer annular space.

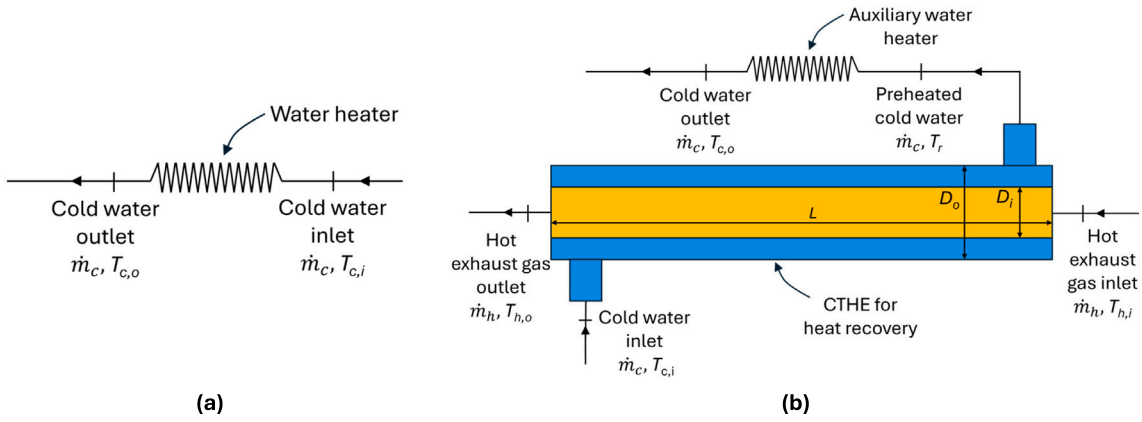

Fig. 1. Schematic of water heating system: (a) without heat recovery; (b) with heat recovery.

$$\overline{U} = \frac{[\log_{10}(\mathrm{Re}_h)]^{b_1} \cdot [\log_{10}(\mathrm{Re}_c)]^{b_2} \cdot \mathrm{Pr}_h^{c_1} \cdot \mathrm{Pr}_c^{c_2} \cdot \left(\frac{\mu_{h,o}}{\mu_{h,i}}\right)^{d_1} \cdot \left(\frac{\mu_{c,o}}{\mu_{c,i}}\right)^{d_2} \cdot \left(\frac{k_h}{D_h}\right) \cdot \left(\frac{k_c}{D_c}\right)}{a_1 \cdot [\log_{10}(\mathrm{Re}_h)]^{b_1} \cdot \mathrm{Pr}_h^{c_1} \cdot \left(\frac{\mu_{h,o}}{\mu_{h,i}}\right)^{d_1} \cdot \left(\frac{k_h}{D_h}\right) + a_2 \cdot [\log_{10}(\mathrm{Re}_c)]^{b_2} \cdot \mathrm{Pr}_c^{c_2} \cdot \left(\frac{\mu_{c,o}}{\mu_{c,i}}\right)^{d_2} \cdot \left(\frac{k_c}{D_c}\right)} \quad (1)$$

Box I.

- Heat is transferred from the exhaust gas to the cold water, raising its temperature to an intermediate value T_r before it enters the auxiliary heater.
- The auxiliary heater then heats the preheated water from T_r to the target outlet temperature $T_{c,o}$, requiring less energy compared to heating from $T_{c,i}$.

3. Mathematical modeling

To accurately predict the performance of the heat recovery concentric tube heat exchanger (HR-CTHE), a comprehensive mathematical model is developed. This model calculates the overall heat transfer coefficient (U) and the heat transfer rate (q) between the hot exhaust gases and the cold water. The approach accounts for variations in fluid properties due to temperature changes and considers both fully developed and developing flow conditions.

3.1. Overall heat transfer coefficient

The overall heat transfer coefficient $\overline{U}$ for the HR-CTHE is determined using a correlation developed by Ali et al. [36] that incorporates the effects of the Reynolds number (Re), Prandtl number (Pr), and dynamic viscosity ratios of both the hot and cold fluids. The correlation is given by (see the Eq. (1) in Box I):
In Eq. (1):

- Re_h and Re_c are the Reynolds numbers for the hot exhaust gases (treated as hot air) and cold water, respectively.
- Pr_h and Pr_c are the Prandtl numbers for the hot and cold fluids.
- $\mu_{h,i}$ and $\mu_{h,o}$ are the dynamic viscosities of the hot fluid at the inlet and outlet temperatures.
- $\mu_{c,i}$ and $\mu_{c,o}$ are the dynamic viscosities of the cold fluid at the inlet and outlet temperatures.
- k_h and k_c are the thermal conductivities of the hot and cold fluids.
- D_h and D_c are the hydraulic diameters of the inner tube and the annular space, respectively. For the inner tube, $D_h = D_i$, and for the annular space, $D_c = D_o - D_i$.
- a_1, a_2, b_1, b_2, c_1, c_2, d_1, and d_2 are empirical coefficients derived in [36].

The coefficients a_2 and b_2, associated with the cold fluid in the annular space, are functions of the hydraulic diameter D_c. They are expressed as [36]:

$$a_2 = g_1 + g_2 D_c + g_3 D_c^2 \quad (2)$$

$$b_2 = g_4 + g_5 D_c + g_6 D_c^2 \quad (3)$$

where g_1 through g_6 are coefficients determined from empirical data. This dependency captures the influence of the annular geometry on the heat transfer characteristics.

The equation for $\overline{U}$ in Eq. (1) is suitable for fully developed flow conditions. However, in many practical HR-CTHE designs, the entry region can be significant relative to the total length. To account for these effects, the overall heat transfer coefficient is adjusted using a correction factor for the length of the heat exchanger (L), as proposed in [36]:

$$U = \overline{U}\left(1 + \alpha L^{\beta}\right) \quad (4)$$

In Eq. (4):

- α and β are empirical coefficients provided in Table 2.
- L is the length of the heat exchanger in meters.
- The exponent β is negative, indicating that as L increases, the correction factor approaches zero, and U converges to $\overline{U}$.

The coefficients in the equations above are optimized for different flow regimes (Laminar–Laminar LL, Laminar–Turbulent LT, etc.) and are summarized in Table 2.

3.2. Heat transfer rate calculation

The heat transfer rate (q) between the hot exhaust gases and the cold water is computed using the counter-flow effectiveness–NTU (ε–NTU) method. Because thermophysical properties (and thus U) depend on temperature, the problem is coupled and solved iteratively. The procedure is as follows [37]:

Table 2
Optimized correlation parameters for different flow regimes.

Param.	LL	LT	TL	TT
a_1	1.985	149.918	0.694	161.665
a_2	$3.686 - 27.768D_c + 156.455D_c^2$	$24.621 - 42.756D_c + 117.214D_c^2$	$204.677 - 152.479D_c - 51.45D_c^2$	$196.981 - 55.884D_c - 40.165D_c^2$
b_1	2.002	4.575	6.199	6.385
b_2	$1.306 + 25.639D_c - 155.886D_c^2$	$6.106 + 2.081D_c - 4.391D_c^2$	$0.975 + 19.641D_c - 116.925D_c^2$	$6.266 + 1.555D_c - 2.077D_c^2$
c_1	0.280	0.228	0.413	0.205
c_2	0.333	0.434	0.382	0.594
d_1	−0.112	−0.117	−0.832	0.053
d_2	1.88	0.442	0.392	−0.032
α	0.846	0.115	0.260	0.018
β	−0.556	−0.406	−0.635	−0.772

1. **Known inputs:** $\dot{m}_h, \dot{m}_c, T_{h,i}, T_{c,i}, A$, geometry, and correlation needed to compute U.
2. **Select initial evaluation temperatures (initialization):** choose initial estimates for mean/bulk temperatures at which properties will be evaluated, e.g.

$$T_{h,m}^{(0)} = T_{h,i}, \qquad T_{c,m}^{(0)} = T_{c,i}, \tag{5}$$

or any reasonable film-temperature guess.
3. **Evaluate properties at iteration $n = 0$:** compute $c_{p,h}^{(0)}, c_{p,c}^{(0)}, k_h^{(0)}, k_c^{(0)}, \mu_h^{(0)}, \mu_c^{(0)}$ at $T_{h,m}^{(0)}$ and $T_{c,m}^{(0)}$ (and any other required properties).
4. **Compute heat capacity rates at iteration n:**

$$C_h^{(n)} = \dot{m}_h\, c_{p,h}^{(n)}, \qquad C_c^{(n)} = \dot{m}_c\, c_{p,c}^{(n)}. \tag{6}$$

5. **Determine $C_{\min}^{(n)}$, $C_{\max}^{(n)}$, and $C_r^{(n)}$:**

$$C_{\min}^{(n)} = \min\left(C_h^{(n)}, C_c^{(n)}\right), \qquad C_{\max}^{(n)} = \max\left(C_h^{(n)}, C_c^{(n)}\right), \quad C_r^{(n)} = \frac{C_{\min}^{(n)}}{C_{\max}^{(n)}}. \tag{7}$$

6. **Compute the overall heat transfer coefficient $U^{(n)}$:** using Eqs. (1)–(4) (with the current properties).
7. **Compute $\mathrm{NTU}^{(n)}$:**

$$\mathrm{NTU}^{(n)} = \frac{U^{(n)} A}{C_{\min}^{(n)}}. \tag{8}$$

8. **Compute the effectiveness $\varepsilon^{(n)}$ (counter-flow):**

$$\varepsilon^{(n)} = \frac{1 - \exp\left[-\mathrm{NTU}^{(n)}\left(1 - C_r^{(n)}\right)\right]}{1 - C_r^{(n)} \exp\left[-\mathrm{NTU}^{(n)}\left(1 - C_r^{(n)}\right)\right]}. \tag{9}$$

9. **Compute the heat transfer rate $q^{(n)}$:**

$$q^{(n)} = \varepsilon^{(n)} C_{\min}^{(n)} \left(T_{h,i} - T_{c,i}\right). \tag{10}$$

10. **Compute outlet temperatures from energy balances (at iteration n):**

$$T_{c,o}^{(n)} = T_{c,i} + \frac{q^{(n)}}{\dot{m}_c\, c_{p,c}^{(n)}}, \qquad T_{h,o}^{(n)} = T_{h,i} - \frac{q^{(n)}}{\dot{m}_h\, c_{p,h}^{(n)}}. \tag{11}$$

11. **Update mean temperatures for the next iteration:** for example,

$$T_{c,m}^{(n+1)} = \frac{T_{c,i} + T_{c,o}^{(n)}}{2}, \qquad T_{h,m}^{(n+1)} = \frac{T_{h,i} + T_{h,o}^{(n)}}{2}. \tag{12}$$

(Any consistent mean/film-temperature definition may be used.)
12. **Convergence criterion:** repeat Steps (3)–(11) for $n = 0, 1, 2, \ldots$ until

$$\frac{\left|q^{(n)} - q^{(n-1)}\right|}{q^{(n)}} < \epsilon_q, \qquad \left|T_{c,o}^{(n)} - T_{c,o}^{(n-1)}\right| < \epsilon_T, \qquad \left|T_{h,o}^{(n)} - T_{h,o}^{(n-1)}\right| < \epsilon_T, \tag{13}$$

where ϵ_q and ϵ_T are prescribed tolerances.

3.3. Pumping power calculations

The pumping power required to overcome pressure losses is calculated based on flow regimes. When the Reynolds number exceeds 4000 (turbulent), empirical correlations developed by Ali et al. [38] are used.

For the hot exhaust gases (turbulent), the dimensionless pumping power is [38]:

$$\frac{\dot{P}_h}{\frac{1}{2}\rho_h D_h^2 V_{inlet,h}^3} = 1.101\mathrm{Re}_h^{-0.333}\left[2.831 + 0.464\left(\frac{L}{D_h}\right)\right] \tag{14}$$

For the cold water (turbulent) [38]:

$$\frac{\dot{P}_c}{\frac{1}{2}\rho_c D_c^2 V_{c,\mathrm{inlet}}^3} = 1.464\,\mathrm{Re}_c^{-0.404}\left[11.543 + 2.036\left(\frac{L}{D_c}\right)\right] \tag{15}$$

In the laminar flow regime, the pumping power is based on the Hagen–Poiseuille equation [39]:

$$\Delta P = \frac{fL}{D}\left(\frac{1}{2}\rho V_{inlet}^2\right) \tag{16}$$

where $f = 64/\mathrm{Re}$. The pumping power is then:

$$\dot{P} = \dot{m}\left(\frac{\Delta P}{\rho}\right) \tag{17}$$

The total pumping power is the sum of both contributions:

$$\dot{P}_{\mathrm{total}} = \dot{P}_h + \dot{P}_c \tag{18}$$

3.4. Assumptions and considerations

The following assumptions are made in the development of the mathematical model:

- The exhaust gas is treated as air with temperature-dependent properties.
- The thermophysical properties of water are functions of temperature and are updated during iterations.
- Heat losses to the surroundings are neglected.
- Steady-state conditions are assumed for the operation of the heat exchanger.
- **Pressure Drop Treatment:**
  - Pressure drops are explicitly calculated and accounted for in the pumping power analysis. For turbulent flows, empirical correlations (Eqs. (14) and (15)) include the influence of pressure drops, while for laminar flows the Hagen–Poiseuille relation is employed.
  - Minor losses (e.g., due to fittings or sudden changes in flow) are neglected.

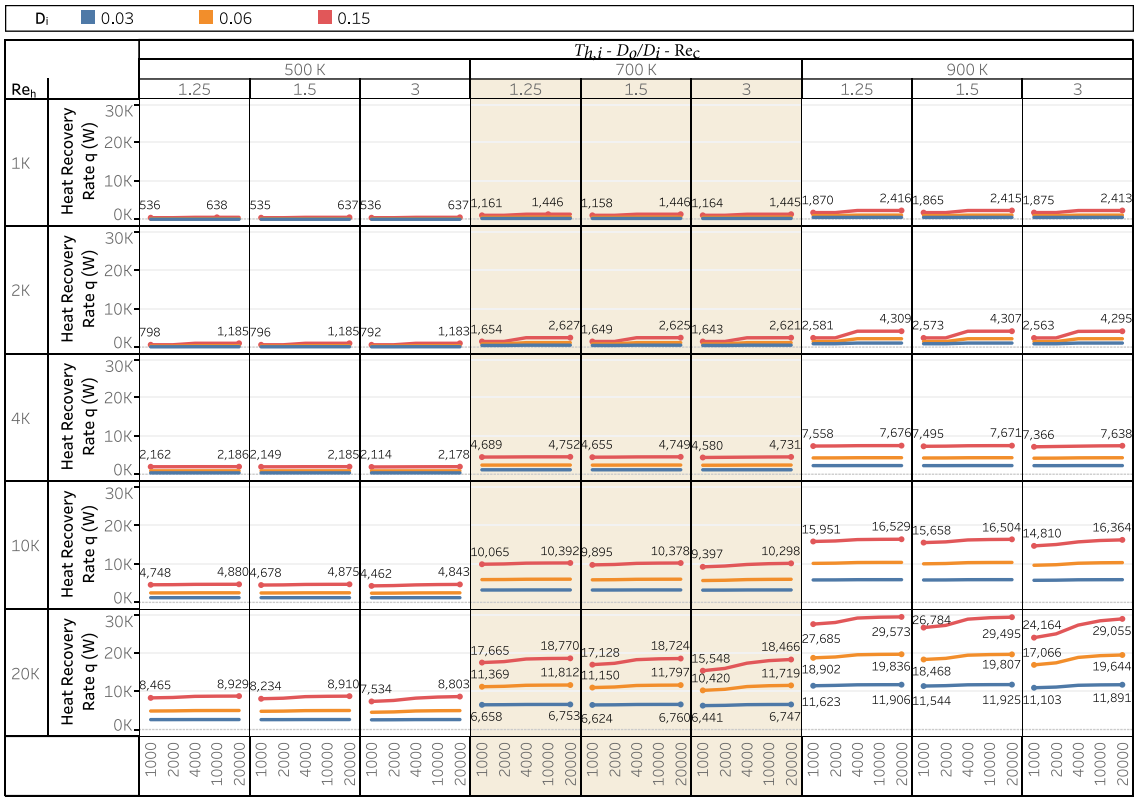

Fig. 2. Heat recovery rate (q in W) as a function of the hot exhaust inlet temperature ($T_{h,i}$), diameter ratio (D_o/D_i), and the cold water Reynolds number (Re_c), presented for various values of the hot exhaust Reynolds number (Re_h). The plots illustrate data corresponding to $T_{h,i}$ values of 500 K, 700 K, and 900 K, with D_o/D_i ratios of 1.25, 1.5, and 3. The inner tube diameters (D_i) of 0.03, 0.06, and 0.15 m are color-coded for distinction. (For interpretation of the references to color in this figure legend, the reader is referred to the web version of this article.)

3.5. Model validation

The reliability of the present 4E analysis relies on the accuracy of the underlying thermo-hydraulic model. The heat transfer and pressure drop calculations in this study utilize specific correlations (Eqs. (1)–(15)) developed by Ali et al. [36,38]. These correlations were derived from an extensive database of over 2700 Computational Fluid Dynamics (CFD) simulations, which were rigorously validated against experimental results for concentric tube heat exchangers.

Statistical analysis in the source studies demonstrated high predictive accuracy for these correlations:

- **Heat Transfer:** The correlation for the overall heat transfer coefficient (U) achieved a median prediction error of 5.18% and an average error of 6.7% across laminar and turbulent regimes [36].
- **Pumping Power:** The friction factor and pumping power correlations showed an average error of less than 2.33% compared to the CFD validation dataset [38].

Consequently, the results generated by the current model are considered to be within the confidence interval of established benchmarks for this specific geometry. Furthermore, the trends observed in the present results — specifically the dependence of heat rate on Reynolds number and the trade-offs between thermal enhancement and pumping power — show qualitative agreement with general trends reported in recent literature on waste heat recovery [33].

4. Results

4.1. Energy analysis

Figs. 2 and 3 summarize the influence of the thermal driving force ($T_{h,i}$), geometry ((D_o/D_i) and D_i), and flow regimes (Re_h, Re_c) on the recovered heat rate (q) and the preheated-water outlet temperature (T_r). In general, q is primarily governed by hot-side convection and available area, whereas T_r is strongly controlled by the cold-side mass flow (residence time) in addition to heat-transfer intensity.

Heat Recovery Rate (q):

- **Hot inlet temperature ($T_{h,i}$):** Increasing $T_{h,i}$ (500→700→900 K) increases q due to the larger temperature driving force; for high Re_h and tight annulus, q rises from $\mathcal{O}(10^4)$ W at 500 K to $\mathcal{O}(2\times10^4–3\times10^40)$ W at 900 K (e.g., $D_i = 0.15$ m, $D_o/D_i = 1.25$, $\mathrm{Re}_h = 20000$).
- **Diameter ratio (D_o/D_i):** A tighter annulus (smaller D_o/D_i) enhances cold-side convection for the same Re_c and generally increases q. For example at $T_{h,i} = 700$ K, $\mathrm{Re}_h = 20000$, $D_i = 0.06$ m, $\mathrm{Re}_c = 1000$, q is higher for $D_o/D_i = 1.25$ than for $D_o/D_i = 3$.
- **Reynolds numbers (Re_h, Re_c):** Increasing Re_h produces the strongest gain in q because it directly lifts the hot-side convection coefficient, which often dominates the overall resistance. By contrast, increasing Re_c increases q more moderately because the cold side is already highly convective compared with exhaust gas.
- **Inner diameter (D_i):** Larger D_i typically increases q by increasing heat-transfer area, even if the hot-side convection is slightly reduced. Consequently, cases with $D_i = 0.15$ m often provide the highest q (e.g., at $T_{h,i} = 900$ K and high Re_h, q for $D_i = 0.15$ m can be more than double that of $D_i = 0.03$ m).

Recovered Water Temperature (T_r):

- **Hot inlet temperature ($T_{h,i}$):** T_r increases with $T_{h,i}$; at 500 K, the preheating is limited (near 280 K), while at 900 K and favorable

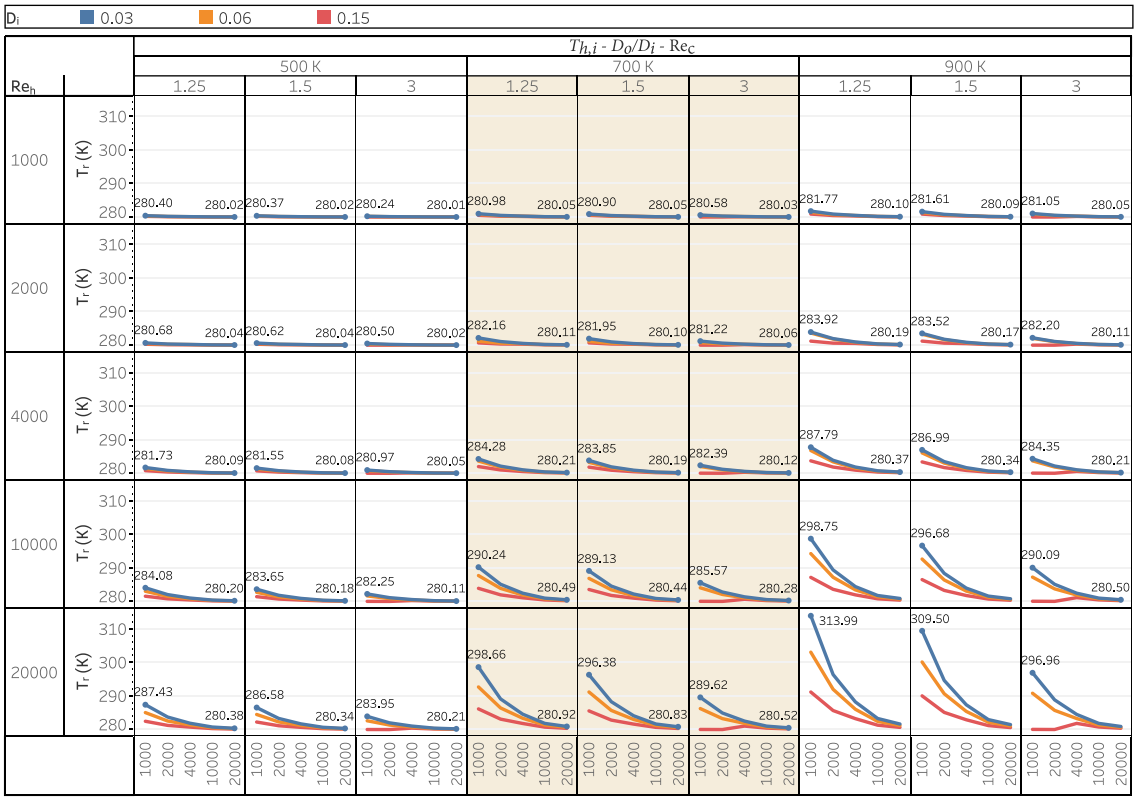

Fig. 3. Preheated cold water temperature (T_r) as a function of the hot exhaust inlet temperature ($T_{h,i}$), diameter ratio (D_o/D_i), and the cold water Reynolds number (Re_c), shown for different values of the hot exhaust Reynolds number (Re_h). The plots represent data for $T_{h,i}$ values of 500 K, 700 K, and 900 K, with D_o/D_i ratios of 1.25, 1.5, and 3. Color coding distinguishes inner tube diameters (D_i) of 0.03, 0.06, and 0.15 m. (For interpretation of the references to color in this figure legend, the reader is referred to the web version of this article.)

conditions (high Re_h, tight annulus, low Re_c), T_r can exceed 310 K.

- **Effect of** Re_c**:** Although higher Re_c can raise q, it typically *reduces* T_r because the recovered heat is distributed over a larger cold-side mass flow rate (shorter residence time), lowering the temperature rise per unit mass.
- **Geometry (D_o/D_i, D_i):** Smaller D_o/D_i (tighter annulus) and smaller D_i generally favor higher T_r at a given Re_c by reducing the required cold-side mass flow and increasing residence time; increasing D_o/D_i tends to depress T_r even when q remains high.

Summary: q is maximized by high $T_{h,i}$, high Re_h, tight annulus, and larger D_i (area-driven). In contrast, maximizing T_r typically requires limiting Re_c (to avoid dilution), using a tighter annulus, and favoring geometries that increase cold-side residence time. Therefore, designs that maximize q do not necessarily maximize T_r, highlighting the need to select operating conditions based on the target (recovered power vs. outlet temperature lift).

4.2. Exergy analysis

This section analyzes the exergetic efficiency (ψ) and exergy destruction ($\dot{E}_{\mathrm{dest}}$) of the HR-CTHE by investigating the influence of key parameters, including Reynolds numbers (Re_h and Re_c), hot exhaust inlet temperature ($T_{h,i}$), inner diameter (D_i), and diameter ratio (D_o/D_i).

Exergetic Efficiency: The exergetic efficiency quantifies the effectiveness of the HR-CTHE in conserving available energy while minimizing losses due to irreversibilities. It is expressed as:

$$\psi = 1 - \frac{\dot{E}_{\mathrm{dest}}}{\dot{E}_{\mathrm{in}}} \tag{19}$$

In this formulation:

- $\dot{E}_{\mathrm{dest}}$ is the rate of exergy destruction caused by irreversibilities, calculated as:

$$\dot{E}_{\mathrm{dest}} = T_0 \dot{\sigma} \tag{20}$$

where T_0 is the reference environment temperature (280 K) and $\dot{\sigma}$ is the rate of entropy generation within the heat exchanger, determined by the entropy balance:

$$\dot{\sigma} = \dot{m}_h(s_{h,o} - s_{h,i}) + \dot{m}_c(s_{c,o} - s_{c,i}) \tag{21}$$

Here, s denotes the specific entropy of the fluids at the inlet (i) and outlet (o).

- $\dot{E}_{\mathrm{in}}$ represents the net rate of exergy input, which corresponds to the reduction in flow exergy of the hot exhaust gases as they pass through the heat exchanger.

The net exergy input is given by:

$$\dot{E}_{\mathrm{in}} = \dot{m}_h \left[(i_{h,i} - i_{h,o}) - T_0(s_{h,i} - s_{h,o})\right] \tag{22}$$

Here:

- $(i_{h,i} - i_{h,o})$ represents the change in specific enthalpy of the hot exhaust gases between the inlet and outlet of the heat exchanger.
- $(s_{h,i} - s_{h,o})$ represents the change in specific entropy of the hot exhaust gases between the inlet and outlet.

Fig. 4 shows that ψ remains relatively low across the parameter space, which is expected for low-to-moderate grade heat recovery where finite temperature differences and flow imbalances generate significant entropy. The main trends are:

Fig. 4. Exergetic efficiency (ψ) of the HR-CTHE device as a function of the hot exhaust inlet temperature ($T_{h,i}$), diameter ratio (D_o/D_i), and the cold water Reynolds number (Re_c), evaluated for various hot exhaust Reynolds numbers (Re_h). The plots present data for $T_{h,i}$ values of 500 K, 700 K, and 900 K, with D_o/D_i ratios of 1.25, 1.5, and 3. Inner tube diameters (D_i) of 0.03, 0.06, and 0.15 m are color-coded for clarity. (For interpretation of the references to color in this figure legend, the reader is referred to the web version of this article.)

- **$T_{h,i}$:** Higher $T_{h,i}$ increases the available exergy and can raise ψ, but the improvement remains limited in absolute value because irreversibilities remain substantial.
- **Re_h vs. Re_c:** Increasing Re_h generally improves ψ by strengthening hot-side convection and reducing the dominant thermal resistance. In contrast, increasing Re_c typically *degrades* ψ because the higher cold-side mass flow intensifies entropy generation and "quenches" the hot stream, lowering the quality of recovered energy.
- **Geometry (D_i, D_o/D_i):** Smaller D_i and tighter annulus (D_o/D_i closer to 1) can yield higher ψ under low Re_c by improving hot-side convection and limiting cold-side mass flow. Increasing D_o/D_i generally reduces ψ because more cold-side flow is required to maintain a given Re_c, amplifying irreversibilities.

Overall, improving second-law performance primarily requires maintaining strong hot-side convection while avoiding excessive cold-side flow rates; this also motivates hot-side enhancement strategies (e.g., inserts/fins/vortex generators) to reduce hot-side thermal resistance and entropy generation.

Exergy Destruction: Fig. 5 indicates that $\dot{E}_{\mathrm{dest}}$ increases with (i) higher $T_{h,i}$ (larger thermodynamic driving force and larger entropy generation), and (ii) higher flow rates, particularly when cold-side flow is pushed to high Re_c. Geometric changes also affect irreversibility through their impact on flow distribution and heat-transfer matching:

- **Effect of $T_{h,i}$ and flow rates:** $\dot{E}_{\mathrm{dest}}$ generally grows with $T_{h,i}$ and increases further as either Re_h or Re_c rises, reflecting stronger entropy generation under larger gradients and higher throughputs.
- **Cold-side intensification penalty:** Very high Re_c can markedly increase $\dot{E}_{\mathrm{dest}}$ due to increased mixing, pressure losses, and stronger thermal "quenching" of the hot stream, which aligns with the observed drop in ψ.
- **Geometric effects:** Larger D_i and/or larger D_o/D_i can increase $\dot{E}_{\mathrm{dest}}$ by altering the hot–cold balance and raising required cold-side mass flow to meet a specified Re_c.

Summary: Figs. 4 and 5 jointly show that higher ψ is obtained only when entropy generation is controlled: strong hot-side convection (high Re_h) must be paired with moderated cold-side flow (avoiding excessive Re_c) and geometries that do not force large cold-side mass flow for a given Re_c. Thus, second-law optimization favors "hot-side strengthening + cold-side moderation" rather than indiscriminately increasing both flow rates.

4.3. Economical analysis

This section evaluates the financial viability of the system by analyzing Annual Savings, Net Present Value (NPV), Discounted Payback Period (DPP), and performing an Exergoeconomic analysis.

Annual Savings: This section analyzes the annual cost savings, expressed in US dollars per year ($/year), as a function of the rate of heat recovery (q). The comparison is made between two water heating systems: an electric water heater and a natural gas water heater. For the electric heater, it is assumed that the energy conversion process is 100% efficient, indicating that all electrical energy supplied is fully utilized as heat without losses. The cost of electricity is set at 0.1685 $/kWh [40]. For the natural gas water heater, a combustion-to-heat conversion efficiency of 90% is assumed, and the price of natural gas is

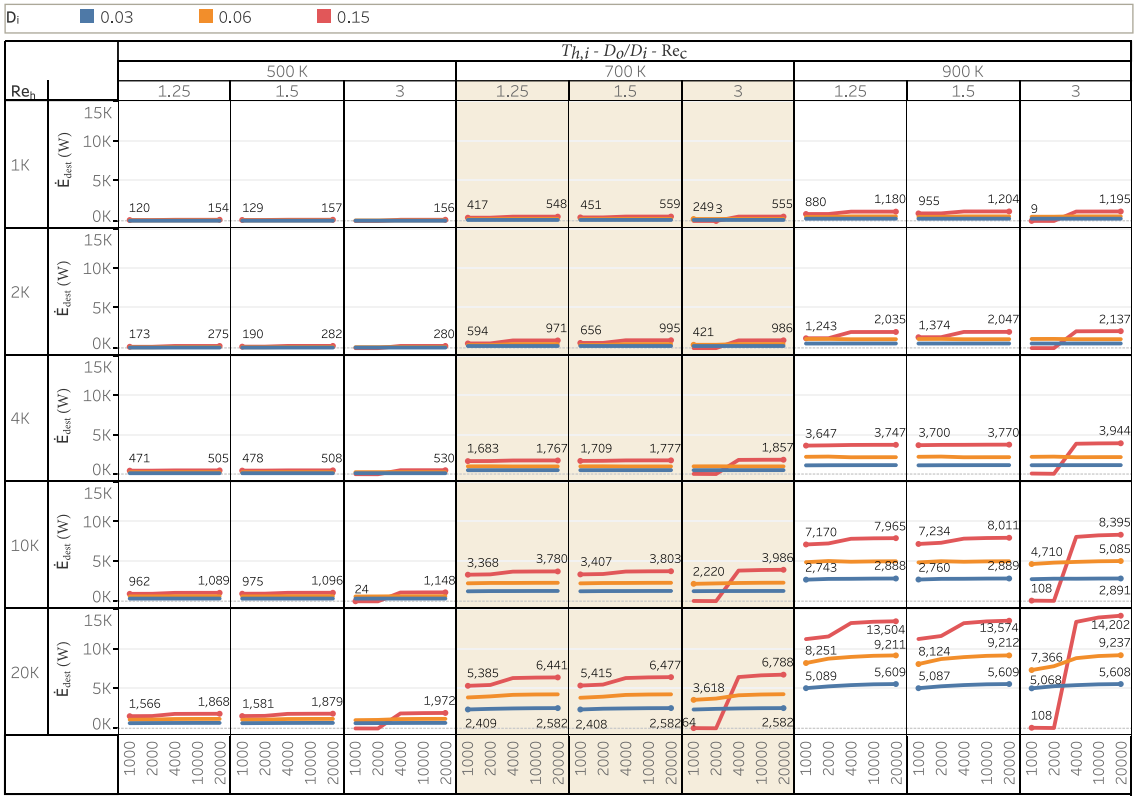

Fig. 5. Exergy destruction rate ($\dot{E}_{\text{dest.}}$) for the HR-CTHE device as a function of the hot exhaust inlet temperature ($T_{h,i}$), diameter ratio (D_o/D_i), and the cold water Reynolds number (Re_c), analyzed for different hot exhaust Reynolds numbers (Re_h). The plots display data for $T_{h,i}$ values of 500 K, 700 K, and 900 K, with D_o/D_i ratios of 1.25, 1.5, and 3. Inner tube diameters (D_i) of 0.03, 0.06, and 0.15 m are represented using color-coded distinctions. (For interpretation of the references to color in this figure legend, the reader is referred to the web version of this article.)

taken as 0.08 $/kWh [40]. The formula used to compute annual savings ($/year) is given by:

$$\text{Annual Savings} = \left(\frac{q}{\eta}\right) k_{\text{price}}\tau \tag{23}$$

In this equation, k_{price} denotes the unit cost of the energy source used for water heating, τ represents the annual operational time (assumed to be 7500 h/year), and η is the efficiency of heat conversion, specified as 100% for the electric heater and 90% for the natural gas heater.

Building upon the trends in q (Section 4.1), Fig. 6 shows that annual savings follow the same hierarchy: higher $T_{h,i}$ and higher Re_h yield the largest savings because they most strongly increase q. Tighter annulus configurations (D_o/D_i closer to 1) generally outperform wider gaps due to improved heat transfer. Finally, the baseline energy source shifts the magnitude: displacing electricity yields substantially larger savings than displacing natural gas for the same recovered heat due to the higher unit price of electricity.

Net Present Value (NPV): The Net Present Value (NPV) is a key financial tool used to evaluate the profitability of an investment over a given period. It calculates the difference between the present value of benefits (cash inflows) and the present value of costs (cash outflows), accounting for the time value of money. By considering that money today holds more value than the same amount in the future, the NPV offers a clear assessment of whether an investment will yield positive returns.

The NPV is determined using the following equation:

$$\text{NPV} = \sum_{t=1}^{N} \frac{\text{Annual Savings} - C_{op}}{(1+r)^t} - C_{in} \tag{24}$$

where:

- Annual Savings refers to the yearly cost reductions achieved through the investment, as derived in Eq. (23) in the previous section.
- r represents the discount rate, accounting for the time value of money and investment risk, set at 10%.
- N is the duration of the investment in years, assumed here to be 10 years.
- C_{op} is the annual operating expense associated with the system, which, for simplicity, excludes maintenance costs.
- C_{in} is the initial capital expenditure required to purchase the heat recovery concentric tube heat exchanger (HR-CTHE).

This equation discounts future savings and costs to their present value and subtracts the initial investment. A positive NPV indicates that the investment's benefits outweigh its costs, suggesting profitability, while a negative NPV implies that the investment may not be financially viable.

The initial investment cost (C_{in}) of the CTHE, constructed with a carbon-steel outer pipe and stainless steel inner pipe, designed to handle pressures up to 4.14 MPa, is expressed as a function of the heat transfer surface area A (in m^2) [41]:

$$C_{in} = 2\exp\left(7.146 + 0.16\ln\left(10.76 \times A\right)\right) \tag{25}$$

The annual operating cost (C_{op}) associated with the power required for pumping to overcome frictional losses is calculated as follows:

$$C_{op} = \frac{1}{\eta}\left(\dot{P}_{total} k_{el}\tau\right) \tag{26}$$

where:

- $\dot{P}_{total}$ is the total pumping power calculated from Eq. (18).
- k_{el} represents the cost of electricity, assumed to be 0.1685 $/kWh.

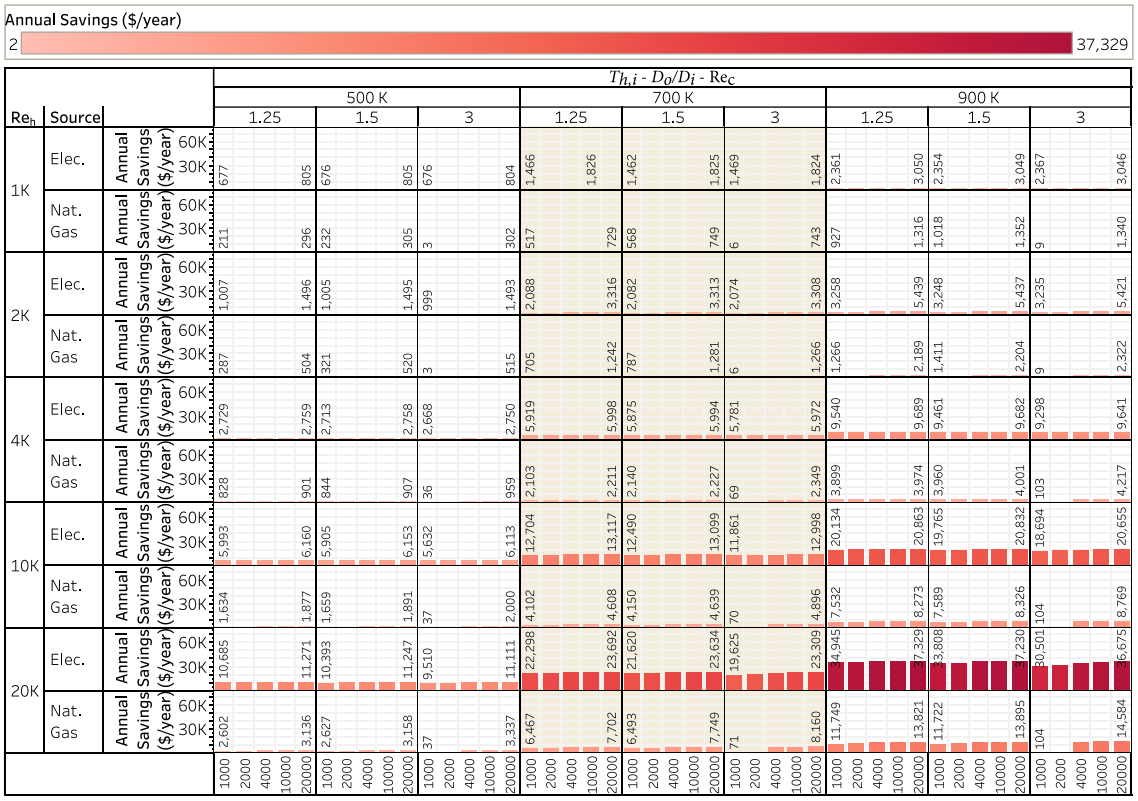

Fig. 6. Annual savings ($/year) as a function of the hot exhaust inlet temperature ($T_{h,i}$), diameter ratio (D_o/D_i), and the cold water Reynolds number (Re_c), evaluated for various hot water Reynolds numbers (Re_h) and two energy sources for water heating: electricity and natural gas. The plots present data for an inner diameter (D_i) of 0.15 m, $T_{h,i}$ values of 500 K, 700 K, and 900 K, and D_o/D_i ratios of 1.25, 1.5, and 3.

- τ denotes the operational time per year, set at 7500 h.
- η is the pump's overall efficiency, assumed to be 0.6.

Fig. 7 indicates that NPV increases strongly with $T_{h,i}$ and Re_h, consistent with their dominant impact on q and hence annual savings. Smaller D_o/D_i ratios tend to improve NPV by enhancing heat transfer and limiting performance losses associated with a wider annulus. Electricity displacement yields higher NPVs than natural gas for the same operating point due to the higher avoided energy cost; consequently, profitability thresholds are reached over a wider region for electricity, while low-$T_{h,i}$/low-Re_h cases can remain non-profitable for natural gas.

Discounted Payback Period (DPP): The discounted payback period serves as a financial indicator that measures the time required to recover the initial capital outlay of a project while incorporating the effects of the time value of money. Unlike the simple payback period, this approach applies a discount rate to future cash flows, thereby accounting for the inherent risks and the opportunity costs associated with the investment. As a result, the discounted payback period provides a more accurate assessment of the timeframe within which the project's initial expenditure is offset by its discounted future net benefits.

The calculation involves the following steps:

- **Discounted Net Savings:** Each year's net savings — that is, the difference between the annual savings and operating costs — is discounted back to its present value. This ensures that future savings are appropriately weighted by the discount rate. Mathematically, this can be expressed as:

$$\text{Discounted Net Savings}_t = \frac{\text{Annual Savings} - C_{op}}{(1+r)^t} \tag{27}$$

Here, t denotes the year of analysis, Annual Savings represents the yearly cost reductions estimated using Eq. (23), C_{op} is the annual operating cost, and r is the chosen discount rate.

- **Cumulative Discounted Net Savings:** The discounted net savings are then aggregated over time until their total reaches or surpasses the initial investment. The cumulative sum over the years is given by:

$$\text{Cumulative Discounted Net Savings}_t = \sum_{i=1}^{t} \text{Discounted Net Savings}_i \tag{28}$$

- **Identifying the Payback Year:** The discounted payback period corresponds to the point when the cumulative discounted net savings equal or exceed the initial investment C_{in}. If this crossover occurs between two specific years, the exact discounted payback period is determined using linear interpolation:

$$\text{Discounted Payback Period} = t - 1 + \frac{C_{in} - \text{Cumulative Discounted Net Savings}_{t-1}}{\text{Discounted Net Savings}_t} \tag{29}$$

Here, t is the year during which the cumulative discounted net savings first surpass the initial investment C_{in}.

By incorporating discounting, this method provides a more nuanced perspective on investment return horizons. A shorter discounted payback period indicates that the project is likely to be more financially appealing and profitable. Conversely, if the cumulative discounted net

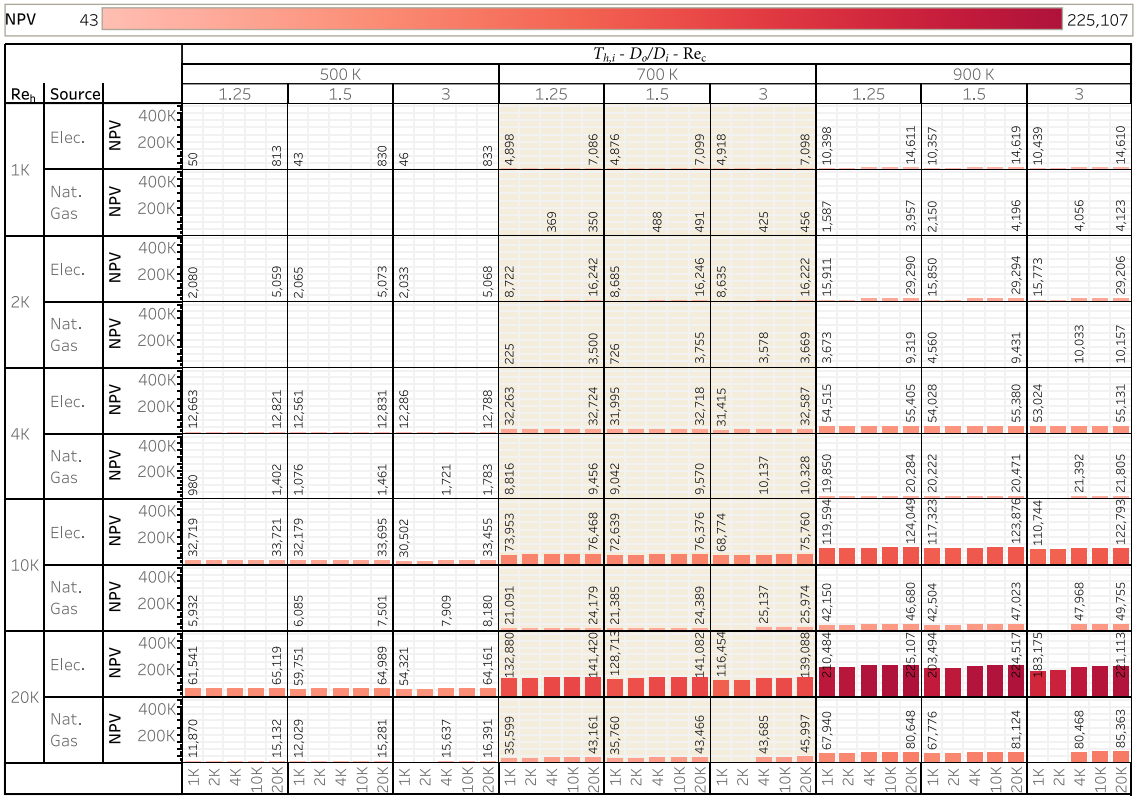

Fig. 7. Net Present Value (NPV) in US dollars as a function of the hot exhaust inlet temperature ($T_{h,i}$), diameter ratio (D_o/D_i), and the cold water Reynolds number (Re_c), analyzed for various hot water Reynolds numbers (Re_h) and two energy sources for water heating: electricity and natural gas. The plots illustrate data for an inner diameter (D_i) of 0.15 m, $T_{h,i}$ values of 500 K, 700 K, and 900 K, and D_o/D_i ratios of 1.25, 1.5, and 3.

savings do not exceed the initial investment within the predefined 10-year analytical window, the project is deemed nonviable under these economic and financial criteria.

Fig. 8 mirrors the NPV trends: DPP shortens markedly at higher $T_{h,i}$ and higher Re_h (higher recovered heat and savings), and it is consistently shorter for electricity displacement than for natural gas. Tighter annulus designs (D_o/D_i near 1) also tend to reduce DPP through improved heat transfer. For low $T_{h,i}$ and low Re_h, especially with natural gas baseline, the payback can exceed the 10-year horizon, indicating non-viable configurations under the adopted assumptions.

Note on Economic Assumptions: It is important to emphasize that the economic results, particularly the extremely short payback periods (<1 year) observed under high-load conditions, are predicated on a continuous operation assumption (τ = 7500 hours/year). This represents a "best-case" scenario suitable for commercial generators or constant-duty applications. For typical domestic residential usage, where hot water demand and engine operation may be intermittent, the effective operating hours would be lower, proportionally extending the payback period. Consequently, the results presented here should be interpreted as the theoretical maximum economic potential of the system under steady-state operation.

Exergoeconomic Analysis: This section presents the application of exergoeconomic analysis to the heat recovery concentric tube heat exchanger (HR-CTHE) and its auxiliary system, as illustrated in Fig. 1(b). Exergoeconomic analysis integrates thermodynamic principles with economic evaluations to assess the cost-efficiency of energy systems by considering both exergy flows and their associated economic costs.

The cost rate balance for the HR-CTHE is derived based on the exergy flow rates and the corresponding costs related to equipment ownership and operational expenses. The total cost rate ($\dot{C}_r$) in $/h at the outlet of the HR-CTHE includes the expenses associated with acquiring and operating the HR-CTHE, represented as $\dot{Z}_{\text{HR-CTHE}}$. By assuming negligible costs for the incoming cold water and the discharged hot exhaust gases, the cost rate balance can be expressed in a simplified form:

$$\dot{C}_r = \dot{Z}_{\text{HR-CTHE}} \tag{30}$$

Here, $\dot{C}_r$ represents the cost rate linked to the exergy of the pre-heated cold water leaving the HR-CTHE.

The term $\dot{Z}_{\text{HR-CTHE}}$ (in $/h) reflects both the initial investment and operating expenses related to the HR-CTHE:

$$\dot{Z}_{\text{HR-CTHE}} = \frac{\text{CRF} \times C_{in} + C_{op}}{\tau} \tag{31}$$

In this expression, τ is the annual operating time of the HR-CTHE, set to 7500 h/year. The Capital Recovery Factor (CRF) is defined as:

$$\text{CRF} = \frac{r(1+r)^N}{(1+r)^N - 1} \tag{32}$$

where r is the discount rate, chosen as 10%, and N is the system's service life, set to 10 years.

When an auxiliary heating system is used to further increase the water temperature to a desired outlet temperature $T_{c,o}$, the cost rate balance must be adjusted. This auxiliary system could be powered by either electricity or natural gas. The cost rate of the final heated water stream ($\dot{C}_{c,o}$) is given by:

$$\dot{C}_{c,o} = \dot{C}_r + c_e \dot{E}_{aux} \tag{33}$$

Here, $\dot{C}_{c,o}$ is the cost rate associated with the exergy of the water exiting the auxiliary heater at $T_{c,o}$, and $\dot{E}_{aux}$ is the additional exergy input required by the auxiliary unit to raise the water temperature from T_r (the temperature after the HR-CTHE) to $T_{c,o}$.

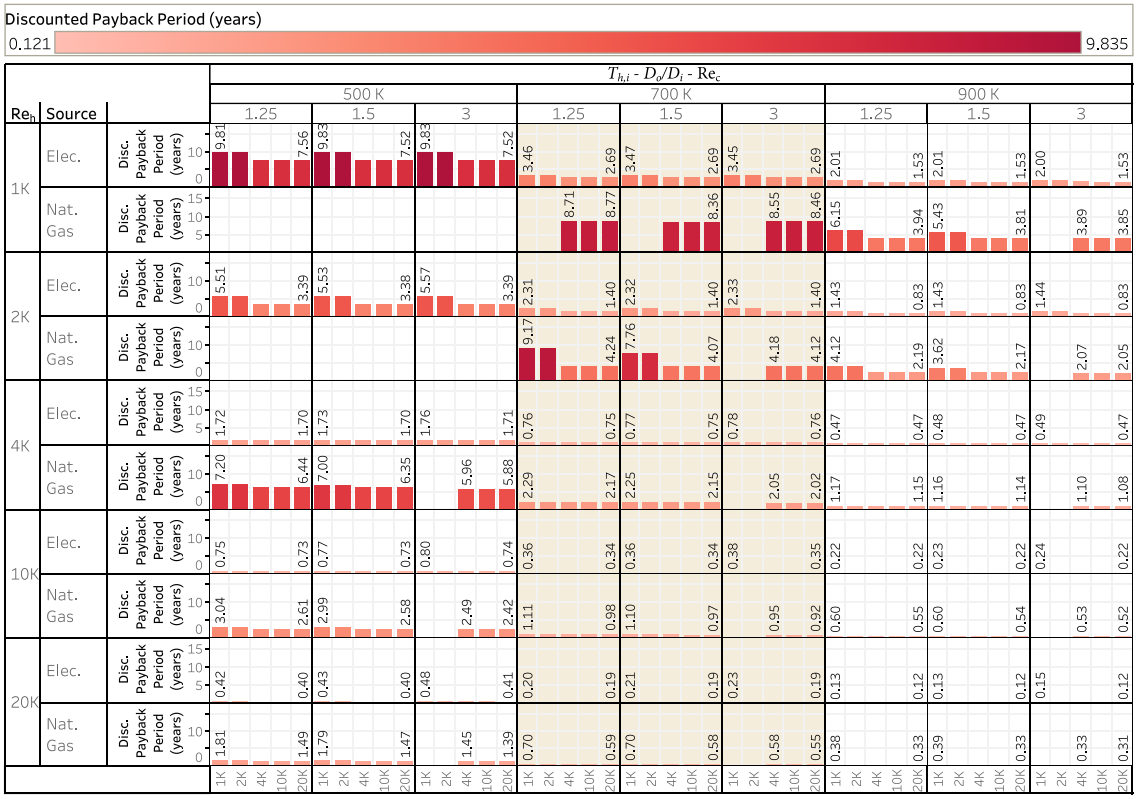

Fig. 8. Discounted Payback Period, expressed in years, as a function of the hot exhaust inlet temperature ($T_{h,i}$), diameter ratio (D_o/D_i), and the cold water Reynolds number (Re_c), evaluated for various hot water Reynolds numbers (Re_h) and two energy sources for water heating: electricity and natural gas. The plots show data for an inner diameter (D_i) of 0.15 m, $T_{h,i}$ values of 500 K, 700 K, and 900 K, and D_o/D_i ratios of 1.25, 1.5, and 3.

For an electric auxiliary heater, the required exergy input $\dot{E}_{aux,elec.}$ can be calculated from the energy needed to elevate the water temperature:

$$\dot{E}_{aux,elec.} = \dot{m}_c C_{p,c}(T_{c,o} - T_r) \tag{34}$$

If the auxiliary heating is provided by natural gas combustion, and assuming the exergy associated with the combustion air is negligible, the exergy input related to the natural gas fuel is:

$$\dot{E}_{aux,NG} = \dot{m}_f e_f \tag{35}$$

In this case, $\dot{m}_f$ is the mass flow rate of the natural gas fuel, and e_f is its specific exergy. The specific exergy is defined as $e_f = \phi \times \text{LHV}$, where $\text{LHV} = 50,000\,\text{kJ/kg}$ and $\phi = 0.99$ [42]. The fuel mass flow rate is determined by:

$$\dot{m}_f = \frac{\dot{m}_c C_{p,c}(T_{c,o} - T_r)}{\eta \times \text{LHV}} \tag{36}$$

Here, $\eta = 0.9$ denotes the combustion efficiency. These relationships ensure that both the cost and performance of the HR-CTHE and its auxiliary heating system are captured in the overall exergy-based cost evaluation.

Fig. 9 shows that the outlet cost rate $\dot{C}_{c,o}$ is primarily driven by (i) the baseline energy source (electricity ≫ natural gas in cost rate), (ii) Re_c (higher cold-side flow increases the heating duty and auxiliary cost), and (iii) the target temperature $T_{c,o}$ (higher setpoints require more auxiliary input). Increasing $T_{h,i}$ reduces the auxiliary burden through increased recovery, but its effect on $\dot{C}_{c,o}$ is comparatively secondary relative to the energy source and Re_c.

The cost ratio $\dot{C}_{ratio}$ in Fig. 10 confirms that the HR-CTHE yields the greatest relative benefit when displacing electricity and when hot-side conditions are sufficiently strong (higher Re_h). For natural gas, profitability margins are smaller (lower avoided unit cost), so favorable performance typically requires higher Re_h and moderated Re_c to ensure that recovery gains are not offset by auxiliary and pumping penalties.

4.4. Environmental analysis

Exergoenvironmental analysis provides a comprehensive framework that unifies thermodynamic efficiency evaluation with a life cycle-based environmental impact assessment. By linking exergy flows with environmental metrics, this approach highlights how changes in system design and operation influence both energy conversion quality and ecological sustainability [43,44]. In the context of heat recovery systems, such as those recovering thermal energy from hot exhaust gas, the exergoenvironmental analysis illuminates the interplay between thermodynamic performance and environmental considerations, including material selection, manufacturing processes, and end-of-life disposal.

At the core of this methodology, the environmental effects associated with each exergy stream are quantified by assigning an environmental impact factor, typically derived from Life Cycle Assessment (LCA) data. LCA, guided by international standards (e.g., using the Eco-indicator 99 method [45]), considers the full life cycle of a component — spanning raw material extraction, manufacturing, operation, and disposal — yielding a holistic measure of its environmental footprint in terms of human health, ecosystem quality, and resource depletion.

For the purpose of this LCA-based assessment, the system boundary is defined to include the manufacturing and end-of-life phases of the

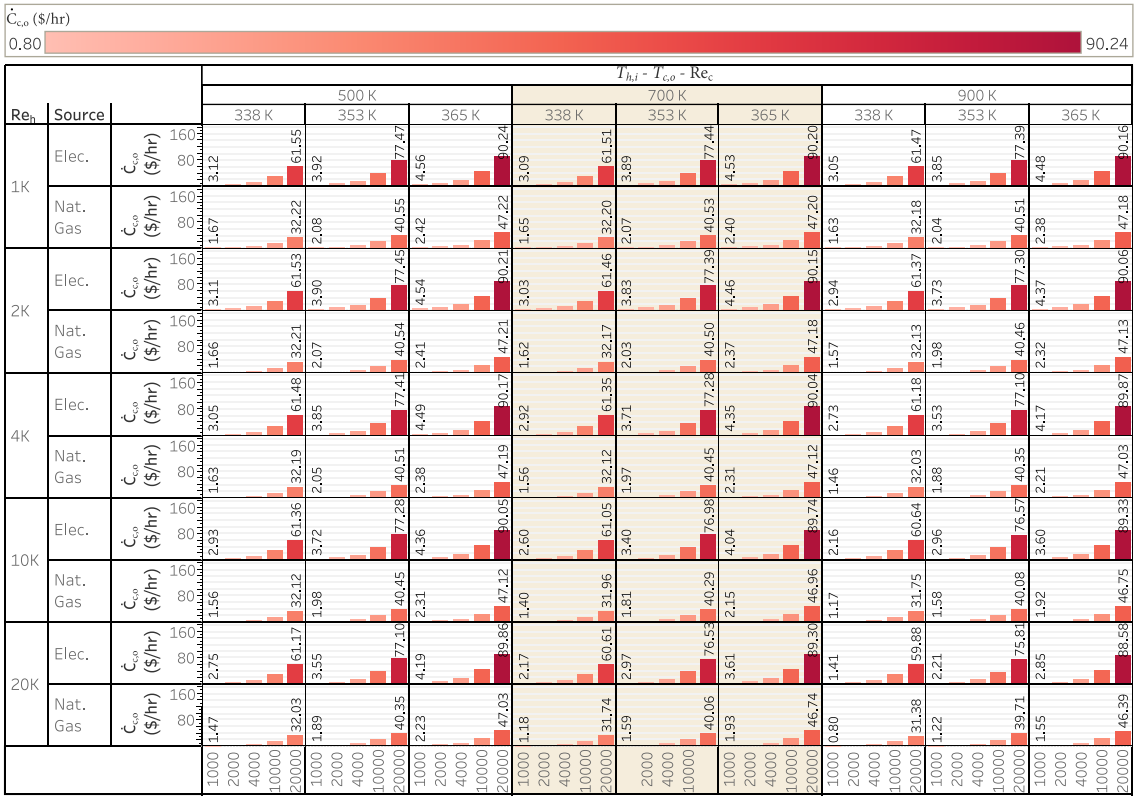

Fig. 9. The cost rate of exergy associated with cold water at the outlet of the auxiliary water heater ($\dot{C}_{c,o}$) integrated with an HR-CTHE. It is plotted as a function of the hot exhaust inlet temperature ($T_{h,i}$), target outlet temperature ($T_{c,o}$), and the cold water Reynolds number (Re_c), for various hot water Reynolds numbers (Re_h) and two energy sources for water heating: electricity and natural gas. The plots display data for an inner diameter (D_i) of 0.03 m, a diameter ratio (D_o/D_i) of 1.25, and hot exhaust inlet temperatures ($T_{h,i}$) of 500 K, 700 K, and 900 K, with target outlet temperatures ($T_{c,o}$) of 338 K, 353 K, and 365 K.

heat exchanger unit itself (materials, processing, disposal) and the operational phase impacts of the auxiliary heater and pumping system. The life cycle of the diesel engine is excluded from the boundary, as its existence and environmental burden are considered independent of the heat recovery system (i.e., the engine operates regardless of whether waste heat is recovered).

The environmental impact balance at the component level can be expressed analogously to the exergy balance:

$$\sum \dot{B}_{\text{out}} + \dot{B}_w = \sum \dot{B}_{\text{in}} + \dot{B}_q + \dot{Y} \tag{37}$$

Here, $\dot{B}$ represents the rate of environmental impact of exergy streams, and $\dot{Y}$ is the component-related environmental impact rate. This $\dot{Y}$ term encompasses three primary contributions:

- **Material production ($\dot{Y}_{\text{Material}}$):** The environmental burdens arising from raw material extraction, refining, and processing into the bulk material.
- **Processing and operational impacts ($\dot{Y}_{\text{Process}}$):** The treatment steps during component manufacturing and the environmental burdens from energy consumption and emissions associated with these processes.
- **Disposal ($\dot{Y}_{\text{DI}}$):** The environmental load or credits associated with the end-of-life phase, including recycling opportunities and waste management.

The environmental impact rate of each exergy stream is calculated using:

$$\dot{B}_i = b_i \dot{E}_i \tag{38}$$

where b_i is the environmental impact factor per unit of exergy (Pts/kWh). In a heat recovery system, this enables direct quantification of how material selection, construction, and operational strategies influence the environmental burden in tandem with thermodynamic efficiency.

For the specific case of a heat recovery concentric tube heat exchanger (HR-CTHE) integrated into the exhaust of a diesel engine, we assume that the environmental impact of the hot exhaust gas is negligible. This assumption is based on the fact that the engine's exhaust stream — which contains the pollutants and emissions — would exist regardless of whether the HR-CTHE is installed. As a result, no additional emissions or pollution are directly attributable to the presence of the HR-CTHE, and the chemical composition and mass flow rate of the exhaust remain unchanged. Thus, the exergoenvironmental balance for the HR-CTHE focuses solely on the impacts associated with the component, its materials, and the auxiliary equipment required to operate it (e.g., pumps):

$$\dot{B}_{c,r} = \dot{B}_{p,c} + \dot{Y}_{\text{HR-CTHE}}. \tag{39}$$

In this equation, $\dot{B}_{c,r}$ is the environmental impact rate at the HR-CTHE's cold-water outlet, and $\dot{B}_{p,c}$ denotes the impact related to the pump driving the cold water through the annular region of the HR-CTHE. This pump impact is evaluated as $\dot{B}_{p,c} = (1/\eta) b_{elec.} \dot{P}_c$, where $b_{elec.}$ is the environmental impact per unit of exergy for the consumed electricity, fixed at 26 mPts/kWh. The term $\dot{Y}_{\text{HR-CTHE}}$ represents the cumulative environmental impact of the HR-CTHE over its entire lifecycle.

Table 3 lists the key material properties used in constructing the HR-CTHE, such as thickness and density. The selection of stainless steel (304/316) for the inner tube, carbon steel (A36) for the outer tube, and polyurethane (PU) foam for insulation each carries distinct environmental implications.

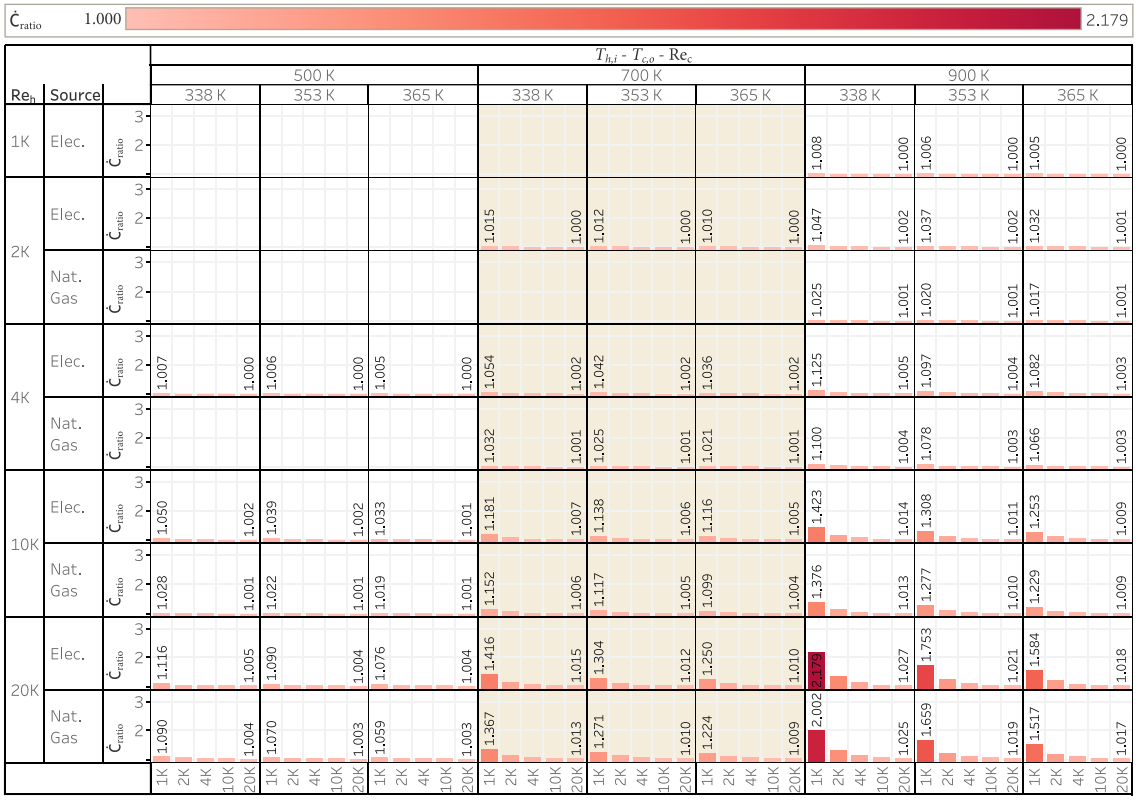

Fig. 10. The cost rate ratio ($\dot{C}_{\text{ratio}}$) as a function of the hot exhaust inlet temperature ($T_{h,i}$), target outlet temperature ($T_{c,o}$), and the cold water Reynolds number (Re_c), analyzed for different hot water Reynolds numbers (Re_h) and two energy sources for water heating: electricity and natural gas. The plots illustrate data for an inner diameter (D_i) of 0.03 m, a diameter ratio (D_o/D_i) of 1.25, and hot exhaust inlet temperatures ($T_{h,i}$) of 500 K, 700 K, and 900 K, with target outlet temperatures ($T_{c,o}$) of 338 K, 353 K, and 365 K.

Table 3
Material properties used in the HR-CTHE.

Material	Thickness (mm)	Density (kg/m^3)
Inner tube: Stainless steel (304/316)	2	8000
Outer tube: Carbon steel (A36)	3	7850
Insulating layer: PU Foam	6	35

The environmental impact factors for the material production, processing, and disposal stages are summarized in Table 4, based on the Eco-indicator 99 methodology [45]. These values, given in mPts/kg or in mPts/m, enable a life cycle-based environmental assessment. They incorporate the energy use during manufacturing (considering the electricity impact factor $b_{\text{elec.}}$) and the credits or burdens associated with end-of-life recycling or disposal. By combining these data with the component's material inventory (Table 3) and its operating conditions, the total exergoenvironmental burden of the HR-CTHE is determined.

Note on the "Process" Entries for Steel Components: For stainless steel (304/316) and carbon steel (A36) in Table 4, the process impact is split into two parts. The first term, expressed in mPts/kg, reflects the environmental impact per kilogram of processed steel and must be multiplied by the total mass of the relevant tube (inner tube if it is made of stainless steel and outer tube if it is made of carbon steel). The second term, shown in parentheses and given in mPts/m, represents additional process-related impacts per unit length of the tube. To obtain the total impact from this length-dependent term, it should be multiplied by the overall length L of the HR-CTHE. This separation ensures that both mass-driven and length-driven contributions to the environmental burden are accurately captured.

At the auxiliary water heater level, the exergoenvironmental balance is given by:

$$\dot{B}_{c,o} = \dot{B}_{c,r} + b_{\text{aux}}\dot{E}_{\text{aux}} \tag{40}$$

where:

- $\dot{B}_{c,o}$ is the environmental impact (EI) rate of the cold water at the outlet of the auxiliary water heater, expressed in millipoints per hour (mPts/h).
- b_{aux} is the EI rate per unit of exergy, which varies depending on the type of water heating used. It is set to 26 mPts/kWh for electrical water heating and 24.21 mPts/kWh for natural gas water heating [45].
- $\dot{E}_{\text{aux}}$ is the exergy input to the auxiliary water heater, which is calculated using either Eq. (34) or Eq. (35), depending on whether the water heater uses electricity or natural gas, respectively.

Figs. 11 and 12 illustrate how integrating a heat recovery concentric tube heat exchanger (HR-CTHE) can reduce the environmental impact (EI) associated with water heating. Fig. 11 presents the environmental impact rate $\dot{B}_{c,o}$ at the cold-water outlet when the HR-CTHE is combined with an auxiliary heater. This is shown as a function of the hot exhaust inlet temperature ($T_{h,i}$), the target outlet temperature of the cold water ($T_{c,o}$), and the Reynolds numbers for hot and cold fluids (Re_h, Re_c). Data are provided for two auxiliary heating sources: electricity and natural gas.

Fig. 12 then focuses on the annual avoided environmental impact, $\Delta\dot{B}_{c,o}$, attributable to integrating the HR-CTHE. This avoided impact is defined as the difference between the EI rate without an HR-CTHE ($\dot{B}^*_{c,o}$) and the EI rate with an HR-CTHE ($\dot{B}_{c,o}$), multiplied by the annual operating hours τ:

$$\Delta\dot{B}_{c,o} = (\dot{B}^*_{c,o} - \dot{B}_{c,o}) \times \tau \tag{41}$$

Table 4
Life cycle assessment impact factors for HR-CTHE components [45].

HR-CTHE component	Material production	Process	Disposal
Stainless steel (304/316)	551 mPts/kg	59 mPts/kg $+(2.4\,b_{\text{elec.}} + 1.05 \times 551)$ mPts/m	−475 mPts/kg
Carbon steel (A36)	86 mPts/kg	18 mPts/kg $+(2.4\,b_{\text{elec.}} + 1.05 \times 86)$ mPts/m	−70 mPts/kg
PU Foam	420 mPts/kg	21 mPts/kg	36 mPts/kg

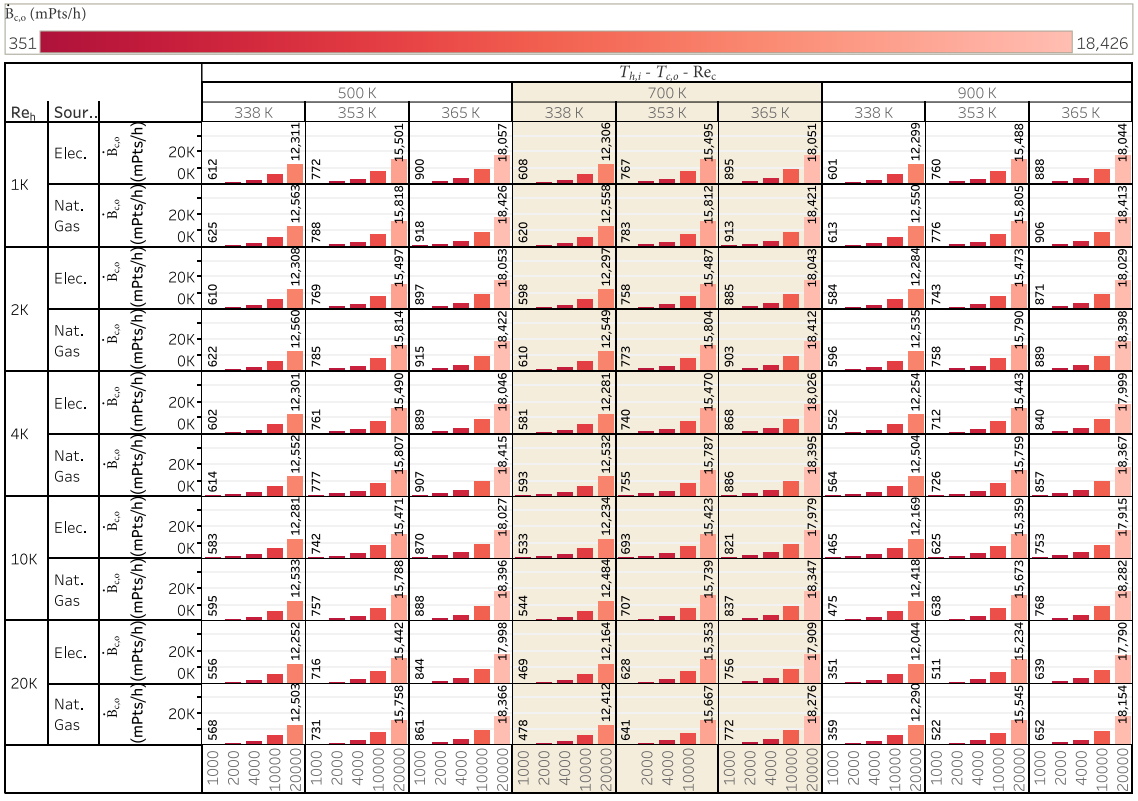

Fig. 11. The environmental impact (EI) rate ($\dot{B}_{c,o}$) as a function of the hot exhaust inlet temperature ($T_{h,i}$), target outlet temperature ($T_{c,o}$), and the cold water Reynolds number (Re_c), evaluated for various hot water Reynolds numbers (Re_h) and two energy sources for water heating: electricity and natural gas. The plots display data for an inner diameter (D_i) of 0.03 m, a diameter ratio (D_o/D_i) of 1.25, and hot exhaust inlet temperatures ($T_{h,i}$) of 500 K, 700 K, and 900 K, with target outlet temperatures ($T_{c,o}$) of 338 K, 353 K, and 365 K.

The observed trends can be summarized as follows:

- **Energy source effect:** Because natural gas heating is modeled at lower efficiency than electric heating, baseline auxiliary demand (and thus $\dot{B}^{*}_{c,o}$) can be higher for natural gas. Consequently, the HR-CTHE often yields a larger avoided impact $\Delta\dot{B}_{c,o}$ in natural-gas scenarios, despite similar EI factors per unit exergy.
- **$T_{h,i}$ and $T_{c,o}$:** Higher $T_{h,i}$ increases recoverable heat and reduces auxiliary demand, thereby increasing avoided impact. Increasing $T_{c,o}$ raises $\dot{B}_{c,o}$ (more heating required), while the *incremental* benefit of the HR-CTHE depends mainly on how much auxiliary energy is displaced by recovery.
- **Re_h and Re_c:** Higher Re_h generally improves recovery and increases avoided impact. Increasing Re_c improves heat transfer locally but raises pumping power and irreversibilities; therefore, very high Re_c can reduce the net environmental benefit. Moderate Re_c often provides the best balance between recovery and auxiliary/pumping burdens.

5. Conclusion and recommendations

This work presented a 4E (energy–exergy–exergoeconomic–exergoenvironmental) assessment of a counter-flow heat-recovery concentric-tube heat exchanger (HR-CTHE) for preheating domestic water using diesel-engine exhaust gas. A broad parametric sweep of operating conditions and geometry was conducted to identify the dominant performance levers and practical design guidelines.

Main conclusions

- **Energy/exergy:** Increasing the exhaust inlet temperature $T_{h,i}$ and hot-side turbulence (Re_h) is the most effective way to raise recovered heat and improve second-law performance, whereas excessively high cold-side flow rates (Re_c) increase irreversibilities and reduce exergetic efficiency.
- **Economics:** Heat recovery is most profitable when displacing electricity (higher unit cost). High $T_{h,i}$, sufficiently large Re_h, and a tight annular gap generally maximize annual savings, NPV, and minimize discounted payback time; natural-gas displacement requires stronger hot-side conditions to remain attractive.

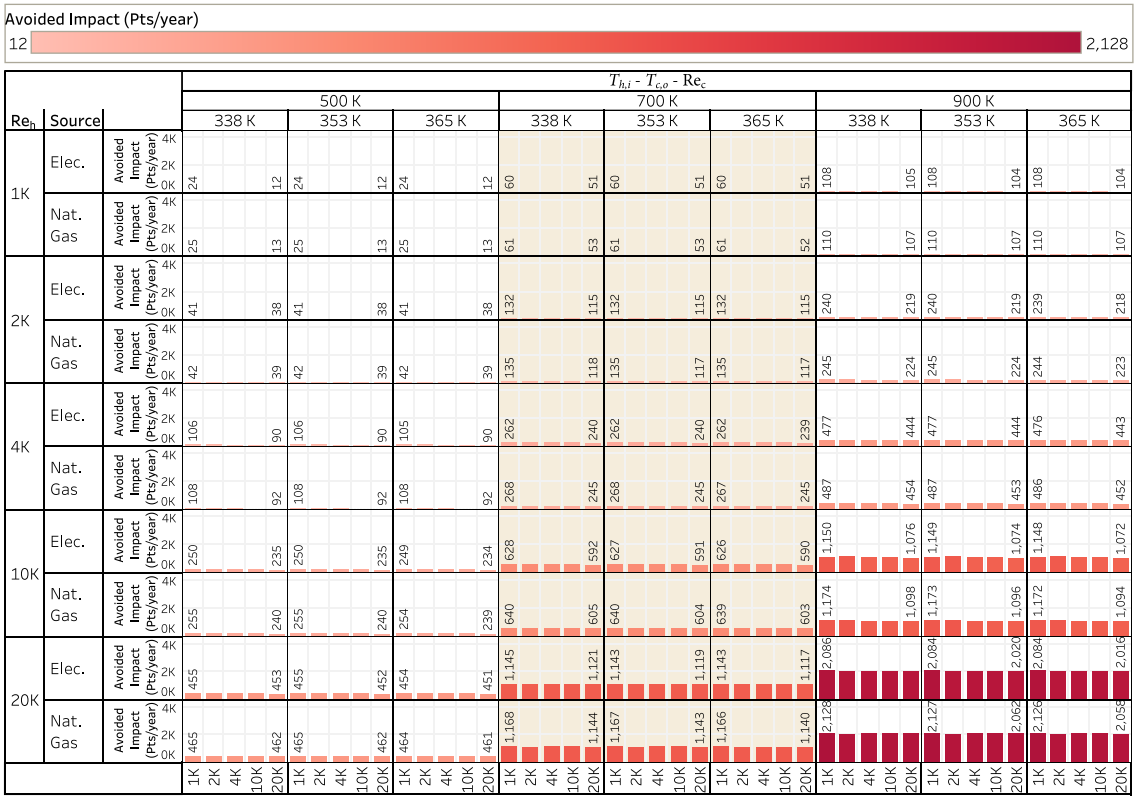

Fig. 12. The avoided environmental impact ($\Delta \dot{B}_{c,o}$) in Pts/year as a function of the hot exhaust inlet temperature ($T_{h,i}$), target outlet temperature ($T_{c,o}$), and the cold water Reynolds number (Re_c), analyzed for various hot water Reynolds numbers (Re_h) and two energy sources for water heating: electricity and natural gas. The plots illustrate data for an inner diameter (D_i) of 0.03 m, a diameter ratio (D_o/D_i) of 1.25, and hot exhaust inlet temperatures ($T_{h,i}$) of 500 K, 700 K, and 900 K, with target outlet temperatures ($T_{c,o}$) of 338 K, 353 K, and 365 K.

- **Environment:** The HR-CTHE reduces life-cycle impact primarily by lowering auxiliary heating demand; the avoided impact increases with higher $T_{h,i}$ and appropriate flow balancing, while very large Re_c can partially offset the benefit due to higher pumping requirements and added irreversibilities.

Design recommendations

- prioritize higher $T_{h,i}$ and turbulent hot-side operation (Re_h) when feasible;
- maintain a relatively small D_o/D_i (tight annular gap) to enhance heat transfer and temperature lift;
- use moderate cold-side flow rates to avoid excessive exergy destruction and pumping penalties.

Future work

Future work will extend the deterministic parametric study by performing global sensitivity analysis and multi-objective optimization to identify Pareto-optimal designs across thermodynamic, economic, and environmental objectives.

CRediT authorship contribution statement

Rassol Hamed Rasheed: Writing – original draft, Validation, Methodology, Investigation, Formal analysis, Data curation, Conceptualization. **Samer Ali:** Writing – original draft, Validation, Methodology, Investigation, Formal analysis, Data curation, Conceptualization. **Ahmed Mohsin Alsayah:** Writing – review & editing, Investigation, Formal analysis. **Mohammed J. Alshukri:** Writing – review & editing, Investigation, Formal analysis. **Saif Ali Kadhim:** Writing – review & editing, Investigation, Formal analysis. **Jalal Faraj:** Writing – review & editing, Validation, Methodology, Investigation, Formal analysis, Data curation, Conceptualization. **Cathy Castelain:** Writing – review & editing, Investigation, Formal analysis, Conceptualization. **Marwan Fahs:** Writing – review & editing, Investigation, Formal analysis. **Mahmoud Khaled:** Writing – review & editing, Project administration, Methodology, Investigation, Formal analysis, Conceptualization.

Declaration of competing interest

The authors declare that they have no known competing financial interests or personal relationships that could have appeared to influence the work reported in this paper.

Data availability

The authors are unable or have chosen not to specify which data has been used.

References

[1] Abed MH, Al-Asadi HA, Oleiwi A, Kadhim SA, Al-Yasiri M, Alsayah AM, Nayyef DR. Improving building energy efficiency through ventilated hollow core slab systems. Case Stud Therm Eng 2024;60:104793.

[2] Riquelme-Dominguez JM, Sempértegui ME, Roldan-Fernandez JM, Serrano-Gonzalez J, Riquelme-Santos JM. Economic assessment of self-consumption and energy communities: Profit distribution insights from a real case study. Energy Convers Manag: X 2025;28:101198. http://dx.doi.org/10.1016/j.ecmx.2025.101198, URL https://www.sciencedirect.com/science/article/pii/S2590174525003307.

[3] Kareem AK, Turki AH, Mohsen AM. Optimization of turbulent flow heat transfer in a 3D cubic shell heat exchanger using non-mixture multiphase nanofluids. J Eng Res 2024.

[4] Allal Z, Noura HN, Salman O, Chahine K. Machine learning solutions for renewable energy systems: Applications, challenges, limitations, and future directions. J Environ Manag 2024;354:120392.

[5] Aboutorabi RSS, Yousefi H, Abdoos M. A comparative analysis of the carbon footprint in green building materials: a case study of Norway. Environ Sci Pollut Res 2024;31(49):59320–41.

[6] Abdoos M, Mobaraki MM, Yousefi H, Noroollahi Y. Evaluating zero-energy strategies in mixed-use buildings: a case study. Futur Energy 2025;4(1):8–18.

[7] International Energy Agency. Heating. 2021, URL https://www.iea.org/energy-system/buildings/heating [Accessed: 13 December 2024].

[8] Odoi-Yorke F. Artificial intelligence for solar water heating systems: A review of global research trends, advances, and future perspectives. Energy Convers Manag: X 2025;28:101378. http://dx.doi.org/10.1016/j.ecmx.2025.101378, URL https://www.sciencedirect.com/science/article/pii/S2590174525005100.

[9] Chen G-R, Liao T-W, Hsieh C-C, Barman J, Huang C-Y, Jeffrey Kuo C-F. Using the taguchi method and grey relational analysis to optimize the parameter design of flat-plate collectors with nanofluids, and phase change materials in an integrated solar water heating system. Energy Convers Manag: X 2025;26:100910. http://dx.doi.org/10.1016/j.ecmx.2025.100910, URL https://www.sciencedirect.com/science/article/pii/S259017452500042X.

[10] Ali S, Dbouk T, Khaled M, Faraj J, Drikakis D. Morphing optimization of flow and heat transfer in concentric tube heat exchangers. Phys Fluids 2023;35(9).

[11] Ali S, Habchi C, Zaytoun H, Khaled M, Dbouk T. Surrogate-based optimization of the attack and inclination angles of a delta winglet pair vortex generator in turbulent channel flow. Int J Thermofluids 2023;20:100473.

[12] Barzantny M, Kostowski W, Nol D, Żymełka S, Kalina J, Stanek W. The silesian paradox: Using coal mines for district heating decarbonization – a case study on waste heat recovery from groundwater and ventilation air. Energy Convers Manag: X 2025;27:101166. http://dx.doi.org/10.1016/j.ecmx.2025.101166, URL https://www.sciencedirect.com/science/article/pii/S2590174525002983.

[13] Pan J, Zhuo Y, Chen W, Yang Z, Wu J, Cai S. Energetic and cost-benefit analysis of multi-heat recovery for enhancing energy management in megawatt-scale PEM fuel cell cogeneration systems. Energy Convers Manag: X 2025;27:101060. http://dx.doi.org/10.1016/j.ecmx.2025.101060, URL https://www.sciencedirect.com/science/article/pii/S2590174525001928.

[14] Alsayah AM, Faraj JJ, Eidan AA. The augmentation of the heat recovery by using evaporative cooling in HVAC applications: Experimental study. Int J Thermofluids 2024;22:100671.

[15] Ali S, Dbouk T, Wang G, Wang D, Drikakis D. Advancing thermal performance through vortex generators morphing. Sci Rep 2023;13(1):368.

[16] Abdelkareem MA, Maghrabie HM, Sayed ET, Kais E-CA, Abo-Khalil AG, Al Radi M, Baroutaji A, Olabi A. Heat pipe-based waste heat recovery systems: Background and applications. Therm Sci Eng Prog 2022;29:101221.

[17] Hammoodi KA, Abdulghafor IA, Kadhim SA, Elsheikh A, Nayyaf DR, mohsin Alsayah A, Hussein KKA, Mohammed ZI. Effect of air layer on PCMs melting process inside a spherical container: A numerical investigation. Results Eng 2024;24:103088.

[18] Turki AH, Kareem AK, Mohsen AM. Heat transfer in a 3D cubic shell heat exchanger with rotating tubes and turbulent flow. Case Stud Therm Eng 2025;66:105757.

[19] Gholizadeh MH, Yousefi H, Hajinezhad A, Abdoos M. Optimization of the economic-technical model for hydrogen production with an approach to utilizing solar power plants and waste-to-energy conversion. Fuel Commun 2025;100144.

[20] Ali S, Faraj J, Khaled M. Heat recovery from hot water drainage: CFD simulation, energy efficiency and exergoeconomic analysis of concentric tube heat exchangers. J Build Eng 2024;98:111034.

[21] Ravichandran A, Diaz-Elsayed N, Thomas S, Zhang Q. An assessment of the influence of local conditions on the economic and environmental sustainability of drain water heat recovery systems. J Clean Prod 2021;279:123589.

[22] Men Y, Liu X, Zhang T. A review of boiler waste heat recovery technologies in the medium-low temperature range. Energy 2021;237:121560.

[23] Rastegarpour S, Mariotti A, Ferrarini L, Aminyavari M. Energy efficiency improvement for industrial boilers through a flue-gas condensing heat recovery system with nonlinear MPC approach. Appl Therm Eng 2023;229:120554.

[24] Kaldeh SN, Yousefi H, Abdoos M, Shirazi MA, Noorollahi Y. Mapping thermal energy storage research in buildings (2020–2025): a bibliometric analysis of trends, themes, and global collaboration. Energy Convers Manag: X 2025;101345.

[25] Shykhaee M, Yousefi H, Hajinezhad A, Abdoos M, Noorollahi Y. Modeling and performance analysis of a solar thermal desalination system using simulation in TRNSYS software. Case Stud Therm Eng 2025;106332.

[26] Mohammaddini S, Yousefi H, Abdoos M, Shirazi MA, Hajinezhad A. Techno-economic simulation of solar flat plate collector systems for building hot water demand supply. Energy 2025;138933.

[27] Zhang X, Rhee K-N, Jung G-J, Kim C. Exploring energy efficiency and savings potential of a horizontal domestic drain water heat recovery system in high-rise apartment buildings. Energy Build 2024;325:115038.

[28] Jia J, Lee WL. Applying storage-enhanced heat recovery room air-conditioner (SEHRAC) for domestic water heating in residential buildings in Hong Kong. Energy Build 2014;78:132–42.

[29] Piotrowska B, Słyś D. Variant analysis of financial and energy efficiency of the heat recovery system and domestic hot water preparation for a single-family building: The case of Poland. J Build Eng 2023;65:105769.

[30] Xie L, Yang J, Yang X, Yu Y, He Y, Hu N, Fan Y, Sun S, Dong F, Cao B. Optimisation of brayton cycle CO2-based binary mixtures: An application for waste heat recovery of marine low-speed diesel engines exhaust gas. Energy 2024;312:133564.

[31] Varshil P, Deshmukh D. A comprehensive review of waste heat recovery from a diesel engine using organic rankine cycle. Energy Rep 2021;7:3951–70.

[32] Wahile GS, Malwe PD, Kolhe AV. Waste heat recovery from exhaust gas of an engine by using a phase change material. Mater Today: Proc 2020;28:2101–7.

[33] Gholizadeh A, Pourfallah M, Gholinia M, Armin M, Languri E. The role of nanofluids and fins in a heat exchanger on waste energy recovery from a diesel engine: An experimental and numerical study. Energy Rep 2022;8:13353–68.

[34] Ni P, Hua R, Jiang H, Wang X, Zhang X, Li X. Thermal flow and thermoelectricity characteristics in a sandwich flat plate thermoelectric power generation device under diesel engine exhaust conditions. Energy 2024;308:132815.

[35] Orido GO, Ronoh EK, Ajwang PO, Gathitu BB. Performance assessment of hybrid recuperative heat exchanger for diesel engine generated exhaust gas. Int J Thermofluids 2023;19:100392.

[36] Ali S, Faraj J, Khaled M. A correlation for U-value for laminar and turbulent flows in concentric tube heat exchangers. Int J Thermofluids 2024;23:100797.

[37] Incropera FP, DeWitt DP, Bergman TL, Lavine AS. Fundamentals of heat and mass transfer. John Wiley & Sons; 2007.

[38] Ali S, Nohra C, Faraj J, Dbouk T, Khaled M. Thermo-hydraulic performance of concentric tube heat exchangers with turbulent flow: Predictive correlations and iterative methods for pumping power and heat transfer. Int J Thermofluids 2024;24:100898.

[39] White FM. Fluid mechanics. McGraw-Hill Education; 2011.

[40] USEnergy Information Administration. Electricity and Natural Gas Prices. 2024, URL https://www.eia.gov [Accessed: 08 December 2024].

[41] Seider WD, Lewin DR, Seader J, Widagdo S, Gani R, Ng KM. Product and process design principles: synthesis, analysis, and evaluation. John Wiley & Sons; 2017.

[42] Dincer I, Rosen M. Exergy: Energy, environment and sustainable development. Elsevier Science; 2012, URL https://books.google.fr/books?id=3QyaMQEACAAJ.

[43] Meyer L, Tsatsaronis G, Buchgeister J, Schebek L. Exergoenvironmental analysis for evaluation of the environmental impact of energy conversion systems. Energy 2009;34(1):75–89.

[44] Keçebaş A, Georgiev AG, Karaca-Dolgun G. Exergy and exergoenvironmental analyses for characterizing heat transfer and pressure drop of any heat exchanger. Energy 2024;290:130170.

[45] Goedkoop M, Sprinsma R. The eco-indicator 99: A damage oriented method for life cycle impact assessment. Methodology report. Amersfoort, Netherlands: Pre Consultants; 2000, URL https://www.pre.nl Accessed online.